Bulletin de la Societe Geologique de France
2015, Volume 186 Issue 4-5 Pages 331-351
http://dx.doi.org/10.2113/gssgfbull.186.4-5.331
http://archimer.ifremer.fr/doc/00283/39423/

Deep crustal structure across a young passive margin from wide-angle and reflection seismic data (The SARDINIA Experiment) - II. Sardinia's margin

Structure crustale d'une jeune marge passive à partir des données sismiques grand-angle et de réflexion (mission SARDINIA) – II. La marge sarde

Afilhado Alexandra [1, 2, 3, *], Moulin Maryline [2, 3], Aslanian Daniel [2], Schnurle Philippe [2], Klingelhoefer Frauke [2], Nouze Herve [2], Rabineau Marina [4], Leroux Estelle [2, 4, 5], Beslier Marie-Odile [6]

[1] ISEL, P-1959007 Lisbon, Portugal.
[2] IFREMER, Dept Marine Geosci, F-29280 Plouzane, France.
[3] Univ Lisbon, Fac Ciencias, IDL, P-1749016 Lisbon, Portugal.
[4] CNRS, IUEM, Domaines Ocean, F-29280 Plouzane, France.
[5] Univ Paris 06, Univ Paris 04, UMR 7193, Inst Sci Terre Paris ISTeP, F-75005 Paris, France.
[6] Geosci Azur, F-06560 Valbonne, France.

* Corresponding author : Alexandra Afilhado, email address : afilhado@dec.isel.ipl.pt

Abstract :

Geophysical data acquired on the conjugate margins system of the Gulf of Lion and West Sardinia (GLWS) is unique in its ability to address fundamental questions about rifting (i.e. crustal thinning, the nature of the continent-ocean transition zone, the style of rifting and subsequent evolution, and the connection between deep and surface processes). While the Gulf of Lion (GoL) was the site of several deep seismic experiments, which occurred before the SARDINIA Experiment (ESP and ECORS Experiments in 1981 and 1988 respectively), the crustal structure of the West Sardinia margin remains unknown. This paper describes the first modeling of wide-angle and near-vertical reflection multi-channel seismic (MCS) profiles crossing the West Sardinia margin, in the Mediterranean Sea. The profiles were acquired, together with the exact conjugate of the profiles crossing the GoL, during the SARDINIA experiment in December 2006 with the French R/V L'Atalante. Forward wide-angle modeling of both data sets (wide-angle and multi-channel seismic) confirms that the margin is characterized by three distinct domains following the onshore unthinned, 26 km-thick continental crust : Domain V, where the crust thins from 26 to 6 km in a width of about 75 km; Domain IV where the basement is characterized by high velocity gradients and lower crustal seismic velocities from 6.8 to 7.25 km/s, which are atypical for either crustal or upper mantle material, and Domain III composed of "atypical" oceanic crust. The structure observed on the West Sardinian margin presents a distribution of seismic velocities that is symmetrical with those observed on the Gulf of Lion's side, except for the dimension of each domain and with respect to the initiation of seafloor spreading. This result does not support the hypothesis of simple shear mechanism operating along a lithospheric detachment during the formation of the Liguro-Provencal basin.

Keywords : Continental passive margin, Crustal structure, Wide-angle seismic, West Sardinian, Transitional domain

Résumé :

Le système de marges conjuguées du golfe du Lion et l'Ouest de la Sardaigne (GLWS), avec son set de données géophysiques important et de toute résolution, représente un endroit unique pour répondre aux questions fondamentales sur le rifting (amincissement de la croûte, nature de la zone de transition continent-océan, le style de rifting et évolution postérieure, connexion entre processus profonds et de surface).

Bien que le golfe du Lion (GoL) ait été le lieu de plusieurs missions de sismique profonde avant le projet SARDINIA (ESP et ECORS expériences en 1981 et 1988 respectivement), la structure crustale de la marge ouest sarde restait inconnue. Cet article décrit les résultats obtenus à partir de l'interprétation et de la modélisation conjointes des profils de sismique grand-angle et de réflexion (MCS) le long de la marge ouest de la Sardaigne, exacts homologues des profils du golfe du Lion, tous acquis durant la mission SARDINIA en Décembre 2006 avec le N/O français L'Atalante.

La modélisation directe de l'ensemble des données (grand-angle et sismique multi-canal) confirme que la marge est caractérisée par trois domaines distincts depuis la croûte continentale non-amincie de 26 km d'épaisseur : Domaine V, où la croûte s'amincit de ~ 26 à 6 km en moins de 75 km environ; Domaine IV où le socle est caractérisé par des forts gradients de vitesse et des vitesses sismiques de 6,8 à 7,25 km/s dans la croûte inférieure, qui sont considérées comme atypiques aussi bien dans le manteau que dans la croûte; et le domaine III composé d'une croûte océanique « atypique ».

La structure observée sur la marge ouest sarde présente une distribution des vitesses sismiques qui est symétrique à celles observées sur le côté du golfe du Lion, à l'exception de la dimension de chaque domaine et des premiers processus d'accrétion océanique. Ce résultat invalide l'hypothèse d'un mécanisme de cisaillement simple, le long d'un détachement lithosphérique, lors de la formation du Bassin liguro-provençal.

Mots-clés : Marge continentale passive, Structure crustale, Sismique réfraction, Sardaigne Occidentale, Domaine transitionnel.

1. Introduction

The study of the deep crustal structure and evolution of passive continental margins is crucial for the understanding of crustal thinning processes and the formation of associated sedimentary basins. Several efforts have been made using physical and numerical modeling to explain the presence and nature of the transitional domain (Brun & Beslier, 1996; Lavier & Manatschal, 2006; Kusznir & Karner, 2007; Huismans & Beaumont, 2008; Aslanian *et al.*, 2009; Huismans & Beaumont, 2011). However, very few studies have been conducted on a conjugate margin pair, especially during the same seismic experiment. Considering that the conjugate margins of the Gulf of Lion and West Sardinia system are both accessible, they represent a natural laboratory for addressing fundamental questions about rifting, i.e., crustal thinning, the nature of the continent-ocean transition zone, the style of rifting and subsequent evolution, and the connection between deep and surface processes.

The main objectives of the SARDINIA seismic experiment (Figure 1B) were:

- to image the deep crustal and upper mantle structure of this young paired margin along exactly conjugate profiles: whilst expanding spread profiles (ESP) were acquired on the Gulf of Lion (Le Douaran *et al.*, 1984; Pascal *et al.*, 1993; Contrucci *et al.*, 2001), no deep information existed on the conjugate Sardinian margin;
- to characterize the nature of the crust of the different domains, and especially in the Ocean-Continent Transition (OCT) zone.
- to test previous hypotheses and discuss the possible origins of these different domains.

Gailler *et al.* (2009) published a first tomographic image, obtained exclusively from first arrivals, of only two conjugate Sardinia profiles (one on each side). The present paper details and corrects their conclusions, presenting the results of the wide-angle seismic modeling using first and secondary arrivals as well as amplitude fit and MSC data, of two profiles perpendicular to the West Sardinia margin. The results of the three wide-angle seismic models of the Gulf of Lion's margin are discussed in the companion paper of Moulin *et al.* (this issue).

2. Geological setting

The West Sardinia margin is the conjugate of the Gulf of Lion margin. This young margin pair forms the Liguro-Provencal basin, created during the convergence between Africa and Europe during the Oligocene (Le Pichon *et al.*, 1971). Its opening occurred in the back-arc region of the south-eastward retreating Apennines-Maghrebides subduction zone (see flow-lines on Figure 1A) and was followed by the opening of the Tyrrhenian Sea (Auzende *et al.*, 1973; Boccaletti & Guazzone, 1974; Réhault *et al.*, 1984; Malinverno & Ryan, 1986; Jolivet and Faccenna, 2000; Jolivet *et al.*, 2006). Furthermore, the Liguro-Provencal Basin is located at the confluence of the eastern end of the Pyrenees and the southern end of the West European Rift system (Rhine Graben, Bresse) (Gorini *et al.*, 1993; Séranne, 1999; Guennoc *et al.*, 2000; Bache *et al.*, 2010). This margin is therefore the result of a complex evolution from the Variscan cycle to present, with successive episodes of rifting (Permo-Triassic, Jurassic, and Oligo-Aquitanian) and compression (Hercynian, Betic, Pyrenean, Alpine, and Apennine orogenies), associated with several phases of magmatism (late Paleozoic, Oligo-Miocene, and Pliocene) (Carmignani *et al.*, 1994; Rollet *et al.*, 2002; Carminati *et al.*, 2012; Geletti *et al.*, 2014).

Cenozoic evolution lead to the creation of oceanic crust in the central part of the Liguro-Provencal basin, starting in the Late Aquitanian (between 23 and 19 Ma), 9 Ma after a short-lived episode of rifting (Gorini *et al.*, 1993; Mauffret *et al.*, 1995; Séranne, 1999; Guennoc *et al.*, 2000; Bache *et al.*, 2010), whereas the neighboring west-southern Valencia Trough stopped its evolution and remained an aborted rifted basin (Watts *et al.*, 1990; Torné *et al.*, 1992; Pascal *et al.*, 1993; Mauffret *et al.*, 1992; Maillard *et al.*, 1992; Collier *et al.*, 1994; Sabat *et al.*, 1997; Ayala *et al.*, 1996; Maillard & Mauffret, 1999).

The post-rift sedimentary evolution is less documented on the West Sardinia margin than on the Gulf of Lion's margin, but seismo-stratigraphic correlations of sedimentary sequences exist for the onshore Oligo-Miocene Sardinia Rift (e.g. Finetti & Morelli, 1973; Ryan *et al.*, 1973; Fanucci *et al.*, 1976; Biju Duval & Montadert, 1977; Cassano *et al.*, 1979; Curzi *et al.*, 1982; Lecca, 1982; Lecca *et al.*, 1986; Thomas *et al.*, 1988; Cassano, 1990 *in* Fais *et al.*, 1996) and offshore margin (Fais *et al.*, 1996; Sage *et al.*, 2005; Sage *et al.*, 2011; Geletti *et al.*, 2011; Geletti *et al.*, 2014).

Hence, the post-rift sequence can be divided into three distinct intervals. The Pre-Messinian sequence was deposited during the Miocene (Réhault *et al.*, 1984; Geletti *et al.*, 2014). The Messinian sequence is related to a major sea level fall in the Mediterranean after its isolation from Atlantic waters (Hsü *et al.*, 1973; Cita & Gartner, 1973; Clauzon, 1973; Ryan, 1976) and includes an erosional surface and the Mobile Salt Unit (MU) (Sage *et al.*, 2005; Cornée et *al.*, 2008; Sage *et al.*, 2011); no detritics or massive evaporites (Lofi *et al.*, 2003; Bache *et al.*, 2009) have been described on the West Sardinian margin. The Post-Messinian sequence (Pliocene-Quaternary), which forms a thin sedimentary cover (< 0.3 ms twt), was mainly supplied by the Sardinia Island (Sage *et al.*, 2011; Geletti *et al.*, 2014).

Most authors (see Moulin *et al.*, this issue, for more details) agree on the definition of five distinct domains, from I to V, inside the Liguro-Provencal basin (Figure 1A and blow-up of Domains III to V on Figure 1B). Domains I and V correspond to the « continental slope domain » of the Gulf of Lion and West Sardinian margin, respectively. Domain III corresponds to the "atypical" oceanic domain and Domains II and IV correspond to the transitional domain on the Gulf of Lion and Sardinian conjugate side, respectively. However, their nature and dimension, especially for Domains II and IV, are still debated. Determining the nature of these transitional domains will help decipher the different processes involved in the formation of continental margins, which eventually lead to seafloor spreading. The lithological composition and affinity of the transitional domains enable us to establish the role and relative importance of the processes active during continental margin formation. It is now recognized that the Moho takes an active part during the formation and evolution of extensional basins (Cloetingh *et al.,* 2013). Observations of Moho imprints, using near vertical seismic reflection and seismic refraction data, onshore and offshore, demonstrate its variability (Mutter & Carton, 2013; Carbonell *et al.,* 2013; Thybo & Artemieva, 2013, Mjelde *et al.,* 2013), and allow us to examine the nature of the deep crust. In this paper, we will focus on the seismic signature of the basement, especially at a deep crustal level and across the transitional zone, in order to provide information on continental crust thinning, exhumation, rock alteration, magmatism, and evolution in relation to seafloor spreading.

3. Data acquisition, quality and processing

During the SARDINIA experiment, CHIRP profiles, bathymetry data, three coincident MCS reflection and wide-angle seismic profiles, and one single MCS reflection profile were collected on the West Sardinia margin. The MCS reflection data was acquired using a 4.5 km 360-trace digital streamer and a tuned airgun array of 8260 cubic inches, which was towed at a depth of 18 – 28 m. A total of 48 ocean bottom seismometers/hydrophones (OBS/OBH) from Ifremer (Auffret *et al.*, 2004), University of Brest, and Geomar Kiel were deployed on the West Sardinia margin, spaced every 7 nmi (~13 km, cf. Figure 1B). In five locations, three OBS were deployed at the same place to ensure the collection of data. One of the seismic profiles perpendicular to the margin (GH) was extended on land by eight land seismic stations (Figure 1B). The airgun array consists of 16 airguns ranging from 100 cubic inch G-guns to 16 L Bolt airguns, with main frequencies centered around 10 – 15 Hz. The airguns were tuned to the first bubble, to enhance low frequencies and ensure deep penetration (Avedik *et al.,* 1993). The shot interval was 60 s at an average speed of 5 knots, which translates to a trace spacing of about 140 – 150 m. The sample rate was 8 ms for the micrOBS, 5 ms for the Geomar, and 4 ms for the OldOBS. A total of 3573 shots (profile GH: 1130, profile G_2H_2: 1214) were fired by the air gun array.

In this paper, we present the velocity models of the two profiles perpendicular to the West Sardinia margin. Profile K7L2, located on the shelf and parallel to the margin, is not presented since most of the deep arrivals are masked by the presence of sea-bottom multiples, preventing an accurate wide-angle model. Profiles GH and G_2H_2, which are 160 and 200 km long transects, respectively (Figure 1), cross the West Sardinia margin from the continental shelf to the “atypical” oceanic crust. Twenty-one ocean bottom seismometers (OBS) were deployed on the G_2H_2 profile, whereas sixteen were deployed on the GH profile. Additionally, the shots on this profile were recorded by eight land seismic stations (OSIRIS stations from the University of Brest and Geosciences Azur) that extended the marine profile ~150 km onshore.

For the two profiles only 33 instruments were used in the wide-angle modeling, since four instruments (OBSS06, 18a, 30a, and 30c) did not record properly.

The direct water wave arrival was used to correct the instruments location, from its deployment position to its location at the seafloor. Instruments in water depth of less than 100 m were not corrected, since the water arrival does not provide enough constraint to ensure relocation. However, the expected drift during the 100 m descent to the seafloor is small, thus not affecting the modeling. Furthermore, instruments that did not record close shots were not corrected if no direct water wave arrival could be picked as a first arrival. The drift of the instruments, even in deep water, never exceeded 200 m. Picking of the onset of first and later arrivals was usually performed without band-pass filtering, however when necessary, different frequency ranges were set for the band-pass filter. Arrivals from larger offsets have a low frequency and high apparent velocity compared to short offset arrivals, so the band-pass frequencies and time reduction velocity were chosen appropriately.

Whilst two stations (SARD05 and SARD08) recorded no data at all (Figure 1), the remaining six land seismic stations positioned on the prolongation of the profile GH recorded high quality data (Figure Annex-1), with clear arrivals from the lower crust and upper mantle. Useful arrivals could be picked up to more than 200 km of source-receiver offset, including arrivals reflected from the Conrad discontinuity and from the Moho (PmP) and refracted in the shallow mantle (Pn) (Figure Annex-1).

Data quality of the seafloor seismic instruments is equally good for the oceanic part (Figure Annex-2) and continental part (Figure Annex-3) on the two dip profiles (Profile GH and G_2H_2). Data exhibit very good quality, with clear reflections from an intra-crustal interface (Figure 4), as well as PmP and Pn arrivals on all stations (Figures Annex-2 and Annex-3, respectively).

Processing of the multi-channel seismic data was performed using the Geovecteur processing package. The processing sequence consisted of: data geometry and binning, noise editing, band-pass filtering (2-8-48-64 Hz), spherical divergence amplitude correction, FK multiple attenuation, external and internal mute, dynamic amplitude, and stacking. Velocity analysis was performed every 200 CDP for the final stack. Finally, a post-stack Kirchhoff time migration using stacking velocities was applied.

4. Wide-angle Modeling

The OBS data were modeled using the ray-tracing algorithm of Zelt and Smith (1992) and the two-dimensional iterative damped least-squares travel-time inversion from the RAYINVR software (Zelt and Smith, 1992). We applied a layer-stripping approach, proceeding from the top of the model (sea-bottom) towards the bottom (Moho). If upper layers were not directly constrained by arrivals from within the layer, they were locally adjusted to improve the fit of the lower layers.

The two-way travel times of the main sedimentary interfaces and the top of basement were picked from the record section of the MCS reflection data, and were converted to depth using the apparent velocity of the refracted phases picked from the OBS data set, in order to build an initial velocity model. The model velocities and depths were iteratively adjusted until an acceptable fit of arrival times from both data sets (OBS and MCS) was obtained (Table 1, 2). In the non-reversed part of the wide-angle seismic profile, in addition to PmP and Pn phases, we also considered the gravity anomaly fit as a second constraint to estimate the thickness and velocity of the crust. The velocity gradients set in the velocity model were further constrained by amplitude modeling, using the asymptotic approach of ray theory to compute synthetic seismic record sections (Zelt & Ellis, 1988).

The model GH is parameterized by eight different layers, while the model G_2H_2 is parameterized by ten different layers: the water layer, four (model GH) and six (model G_2H_2) sedimentary layers, two crustal layers, and one lithospheric mantle layer (Figure 2). Depth and velocity nodes define each layer. Water velocities, set when correcting OBS locations for drift from the deployment position, are 1.53 km/s on profile GH, whereas a velocity gradient of 1.53 – 1.54 km/s provided a better fit than a constant velocity on profile G_2H_2. Depth nodes of the seafloor and sedimentary layers are set from the picking of sediments mega-sequences boundaries from the MCS reflection profile, at intervals that depend on interface topography as observed on the MCS record section. On land, topography was included with the altimetry measurements at each land-station. The depth nodes that shape the intra-crustal interface and the Moho were set according to the apparent velocity fluctuation of the phases that reflect from and refract across the respective interface, when they are not related to the sedimentary section or to the top of basement topography.

For the GH model, the sedimentary layers have top and bottom seismic velocities of 1.95 – 2.9 km/s (Post-Messinian), 3.8 – 4.2 km/s, 4.2 – 4.4 km/s (both Messinian), and 4.5 – 4.8 km/s (Pre-Messinian) (Figure 2A). Between -180 and -80 km, the second Messinian layer presents a velocity inversion that systematically imprints the data by a step back of the phases that turn in the Pre-Messinian layer (Figures Annex-2 and Annex-4). We modeled this layer with velocities of 3.5 – 3.6 km/s, instead of 4.2 – 4.4 km/s for the rest of the model. Below, in the Pre-Messinian layer, the velocities remain lower (4.5 – 4.6 km/s, instead of 4.5 – 4.8 km/s) in the same area (-180 and -90 km). This zone matches the abyssal plain, after the necking zone. This velocity inversion is not observed on the conjugate Gulf of Lion margin (Moulin *et al.,* this issue). The GH model is comprised of three basement layers: upper crust, lower crust, and a lithospheric mantle layer (Figure 2A). The upper crust shows velocities between 5.3 – 6.3 km/s on the distal part (between -180- and -20 km) and 6.0 – 6.4 km/s on the proximal part of the profile, which are well resolved except in the extremities of the profile (see discussion ahead - point 5). The lower crust is characterized by velocities between 6.3 and 6.9 km/s in the distal part (-180 to -130 km), 7.0 and 7.2 km/s in the central part (-120 to -80 km) and finally 6.5 and ~6.7 km/s in the most proximal part of the profile. The lithospheric mantle is characterized by velocities ranging between 8.0 and 8.4 km/s along the entire model profile. The high velocity at the base of the lithospheric mantle layer (8.4 km/s) is required to explain the high apparent velocity and strong amplitude of the Pn, especially on the land seismic stations (Figure Annex-1). A second lithospheric mantle layer, with a constant velocity and parallel to the Moho, though18 km deeper, is necessary in order to keep the velocity gradient fixed (Figure 2A).

For the profile G_2H_2, the sedimentary layers have top and bottom seismic velocities of 2.0 – 2.1 km/s, 2.4 – 2.75 km/s, and 3.3 – 3.5 km/s (Post-Messinian), 3.85 – 4.1 km/s and 4.2 – 4.7 km/s (both Messinian), and 4.35 – 4.5 km/s (early Messinian and Pre-Messinian) (Figure 2B). This profile also shows a velocity inversion in the early Messinian. The inversion is present between 0 and 70 km (Domain III), which also matches the abyssal plain after the necking zone. Two large domains are distinguished in the sedimentary basin, to the east and to the west of ~100 km, which approximately corresponds to the necking zone (Figure 2B). The G_2H_2 model is comprised of three basement layers: upper crust, lower crust, and a lithospheric mantle layer (Figure 2B). The upper crust in the extremities of the profile is characterized by velocities of 5.1 – 5.5 km/s in Domain III (on the western part) and smoothly increasing from 5.65 – 6.4 km/s to 6.2 – 6.4 km/s across Domain V and the Hinge Zone (on the eastern part). In the center of the profile the upper crust velocity varies from the above velocities, at the limits of Domain IV, to 5.1 – 6.3 km/s in the center, where the velocity gradient reaches its maximum (Figure 2B). The limit between Domains IV and V is marked by an abrupt change of the upper crust velocities. Lower crust velocities change from 6.5 – 7.1 km/s in the western part of the profile to 6.5 – 6.7 km/s on the eastern extremity. In the region immediately west of the necking zone we modeled an important increase of the velocity and velocity gradient at the deep crust – the lower crust velocity increases to 6.8 – 7.25 km/s, which is accompanied by an increase of the velocity at the bottom of the upper crust (Domain IV, Figure 2B). Finally, the lithospheric mantle velocity, constrained by Pn arrivals, varies from 7.95 km/s (in the west) and 8.0 km/s (in the east), to less than 8.1 km/s at its maximum penetration depth.

In Domain Va and the Hinge Zone (profile G_2H_2, Figure 2B) we observe a very strong post-critical PmP (Figure 3A, 95 – 140 km model distance), while the pre-critical PmP seems to be absent (Figure 3A, 140 – 160 km) or is very weak and discontinuous (Figure Annex-3A). The sudden onset of the post-critical PmP suggests that the crust-mantle transition may be better modeled by (i) a thin layer with a high velocity gradient, rather than (ii) a velocity contrast across an interface. We tested both hypotheses, including and excluding the critical Pn (head-wave). The best fit of the observed amplitudes for hypothesis (i) was obtained considering an increase of 6.8 to 7.95 km/s in a 0.2 km-thick layer, representing the Moho. This model can predict the onset of a very strong PmP at ~140 km (~40 km source-receiver offset), as well as its amplitude variations with offset (Figure 3B). Although hypothesis (ii) also predicts a very strong PmP, it does not account for the amplitude decrease observed at ~125 km (~55 km source-receiver offset), when we exclude the critical Pn of the computation of the synthetic record section (Figure 3C). If the critical Pn is included in the computation of the synthetic record section (Figure 3D), the observed amplitude fluctuation with offset of the post-critical PmP is equally well reproduced by both alternative models (Figures 3B and D). Therefore, we cannot discard one of the hypotheses based on the post-critical fit of amplitude. Furthermore, since the computed amplitude of the pre-critical PmP for hypothesis (ii) is small, it may be argued that it is not identified because it is below the noise level. Both hypotheses are thus acceptable, providing that head-waves are generated for case (ii), with a velocity contrast across the Moho of 6.8 km/ over 8.0 km/s.

5. Error Analysis

The fit between predicted arrival times and travel-time picks is part of model evaluation (Figures 4 to 6). A first quantifier for the fit is expressed in terms of the $\chi 2$, defined as the root-mean-square travel-time misfit between observed and calculated arrivals, normalized to the picking uncertainty. Estimated picking uncertainties were 75 ms for all arrivals. The number of picks, RMS travel-time residuals, and the χ^2-error for all phases are listed in Tables 1 – 2 (for model GH and G_2H_2, respectively).

A second quantifier for model evaluation is the ray coverage, which allows us to distinguish between the imaged and unconstrained regions of the model, usually given by two-point ray-tracing between source and receiver. We present a global view of ray coverage and arrival time fit for different depth levels (sediments, basement and Moho, and mantle) (Figures 4 and 5), together with a few examples at selected seismic stations, that gives a more detailed view of ray coverage and arrival time fit (Figure 6). On profile GH, ray coverage is good, except for the sedimentary layers. Only near-offset reflected phases from the top of the different sedimentary layers are identified, due to the presence of salt diapirs. All rays arriving at the land seismic stations emerge at very steep angles and therefore do not allow us to model the shallow sedimentary structures on land. On profile G_2H_2, ray coverage is very good, except in the eastern part of the model (between 120 and 200 km model distance), where the sedimentary layers are not well imaged due to its complex morphology. However, crustal layers and lithospheric mantle are well imaged along the entire profile.

Additional information about the velocity model can be gained from the model resolution (Figure 7) (Zelt & Smith, 1992) which indicates how well a model parameter is constrained by the data. A high-resolution value for a particular model velocity or depth corresponds to a high confidence in its value. The resolution of one particular velocity node depends on the relative number and angular distribution of rays constraining that node. Homogeneous layers, which are parameterized with a low number of nodes, can be well resolved by relatively few rays passing through the layer, whereas heterogeneous layers, parameterized with many velocity nodes, require a large number of rays passing through in order to achieve a similar resolution level. Velocity nodes having resolution greater than 0.5, corresponding to the gray and yellow areas on the model, are considered well resolved (Figure 7). Only a few regions along the profiles show a resolution smaller than 0.5, which is considered poorly resolved, and those are marked in red. They correspond to the extremities of the profiles. In particular, the velocities of the upper crust in profile GH between -150 and -90 km are not resolved, due to the absence of turning or reflected rays from the upper crust in this region (Figure 4B). Similarly, the resolution of depth nodes, depicted as squares of area proportional to resolution (Figure 7), is greater than 0.5 everywhere, except for the Conrad discontinuity, showing that the geometry and interface depths of the layers are well resolved.

We also performed a smearing check among model parameters; computing local spread functions from the out-of-diagonal elements of the resolution matrix (Afilhado *et al.*, 2008). We verified that the smearing of velocities and depths decreases with increasing resolution, always remaining at acceptable levels of smearing with respect to the other parameters (local spread function values less than 2) for well-resolved parameters. The only exception is the velocity of the salt layer in profile G_2H_2, which is well resolved according to its resolution value, but with its local spread function being comparatively high, indicating some level of smearing as compared to other parameters.

6. Comparison with seismic reflection data

Figure 8 displays the good correlation between the depth to two-way travel-time conversion of the velocity models with the MCS seismic profiles. Note that only reflectors correlated with reflected phases identified in the OBS data, and therefore necessary for the wide-angle modeling, were included, avoiding over-parametrization of the model and thus reducing the level of under-determination of the inversion. On the G_2H_2 profile, six main sedimentary layers were identified and included into the model, whereas on profile GH there are four sedimentary layers included into the model. The difference came from the Plio-Quaternary sediments, where it was possible to differentiate two separate layers, rather than a thicker layer with a strong gradient.

Although the depth and velocities of the crustal layers and lithospheric mantle were modeled exclusively from the OBS data, we obtain a good agreement of the velocity model interfaces with deep reflectors identified in the MCS record section, especially for a strong energetic reflector identified at a depth of around 8 s twt and interpreted as the Moho in Domains III and IV (Figure 8). Nevertheless, in Domain IV the relationship between velocity model interfaces and deep reflectors is not as evident as in the Gulf of Lion, i.e, the strong and chaotic reflector, which corresponds to the basement, is not as clear as on the conjugate side (see Figure 8 of Moulin *et al.*, this issue). We also do not observe the highly stratified Miocene unit at the top of the basement on the West Sardinia margin. These differences may be related to the presence of a thicker salt layer in this area.

It is also worth noting that MCS data do not show any feature correlative with the so-called “T-reflector” observed on Gulf of Lion margin (De Voogd *et al.*, 1991). This feature has been described as a landward deep detachment, related to exhumation of the lower continental crust (Séranne *et al.*, 1995; Séranne, 1999). It separates the top of a high velocity zone (Pascal *et al.*, 1993) composed by gabbros or granulites, from the pinch-out of the lower continental crust (Moulin *et al.*, this issue). Instead, the wide-angle seismic data show that the lower continental crust velocities increase from 6.5 – 6.7 km/s to 6.8 – 7.25 km/s, a crustal velocity structure not typical of continental crust, nor of oceanic crust. It corresponds to the initiation of the anomalous velocity zone, which is limited to Domain IV. On Profile G_2H_2, the upper crust is marked by a sharp lateral change in the velocities and is followed by an increase of the bottom velocity from 5.5 to 6.3 km/s (Figures 2 and 9). This heterogeneity may be the signature of a fault or a lithological contact between the granitic upper continental crust to the East and a different lithology to the West, which we discuss in the next section.

7. Discussion

Our study highlights for the first time, along two velocity-depth profiles, the sedimentary section, deep crustal structures, and crust-mantle boundaries of the West Sardinian margin. The main difference between the two velocity-depth profiles relates to their obliquity with the NE- and NW-trending Hercynian structures (Fais *et al.*, 1996 in Sage *et al.*, 2005). The latter also controlled the onshore Oligo-Miocene Sardinia Rift depicted in the topography (Figure 1). One major transfer fault intercepts profile G_2H_2 between Domains V and IV (Figure 9) while it crosses profile GH within Domain V. Transfer faults may thus induce an abrupt seaward thinning of the continental crust. The 3D character of the continental margin in the non-volcanic segment of the Gulf of Aden was also interpreted to be the result of segmentation of the margin (Watremez *et al.*, 2011). The abrupt thinning observed on profile G_2H_2 would thus be related to a specific feature, while the more regular thinning observed along profile GH would probably be more representative of the style of thinning of the Sardinia margin.

Sedimentary layers. On the GH profile, the sedimentary section thickens from 0.5 km (at OBSS 26) near the shoreline to 4.8 km (at OBSS 14) around -150 km, a thickness far below what it is observed on the Gulf of Lion (7.5 km maximum in the center of the basin). The sedimentary thickness in the abyssal plain is more or less constant (+/- 4 km) and is comprised of three main layers (see Geological Setting). This study confirms the existence, just above the basement, of high velocities (4.4 – 4.8 km/s) in the Miocene sequence, consistent with the high values (5.0 – 5.4 km/s) observed on the Gulf of Lion's side by Pascal *et al.* (1993). This layer reaches a thickness of around 2 km and is present on the entire profile. Following Moulin *et al.* (this issue), it could correspond to Mio-Tortonian to Aquitanian deltaic deposits as defined by Bache *et al.* (2010).

Crustal structure. Four main regions on the West Sardinian margin (Figures 1 and 2) can be distinguished on the base of the seismic facies of their basement (Figures 8 and 10), their seismic velocity structure (Figures 9 and 11), and their density structure, as previously stated by Gailler *et al.* (2009). These four regions look equivalent to those described by Bache *et al.* (2010) and Moulin *et al.* (this issue) on the Gulf of Lion side, except for their dimensions, as regions IV and V are smaller than the conjugate regions II and I:

A) An unthinned continental domain: The presence of a homogeneous continental crust, which reaches a thickness of about 27 km in the onshore domain, is clear from the wide-angle seismic data set (25 – 80 km model distance on profile GH) and was modeled by land seismic stations, PmP and Pn arrivals (Figure 2), and gravity anomaly fit. The crust is represented by two layers of roughly similar thickness (11 and 15 km in the onshore domain), with velocities of 5.9 – 6.4 km/s and 6.5 – 6.7 km/s, respectively. The presence of an upper-lower crust velocity step, called the Conrad discontinuity, is required by the wide-angle seismic data (Figures Annex-1 and Annex-3 (115 – 130 km)), since reflected phases are continuously observed on the land seismic stations (Figure 6A) and on the OBS (Figures 6C, E, G) in both profiles (Figures 4B and 5B). The lower crust velocity was mainly constrained by the strong post-critical PmP phases (Figures Annex-1 and 3), and a few refracted weak phases (Figures 4B, 6E, and 5B). The two layers have a low velocity gradient (Figures 11A and D), in good agreement with the relatively weak Pg phases observed in the continental domain (Figures Annex-3 (150 – 170 km) and 3 (120 – 160 km)). Such crustal thickness, velocity, and velocity gradient values are typical of continental crust (Christensen & Mooney, 1995; Figures 11A and D) and similar to previous results from the European Geotraverse (Galson & Mueller, 1987; Ansorge *et al.*, 1992).

B) The "continental slope domain" can be divided into two contrasting sub-domains: the Hinge Zone and Domain V (Figures 2, 8, and 9): i) The Hinge Zone (0 – 25 km (GH) / 170 – 200 km (G_2H_2)) marks the landward zone of crustal thinning, from 25 to 20 km, mainly in the upper crust; ii) Domain V is the main crustal thinning zone (-60 – 0 km (GH); 110 – 170 km (G2H2)), mainly focused in the lower crust; the Moho steeps gently beneath Domain Va, whereas beneath Domain Vb (-60 – -35 km (GH); 110 – 135km (G_2H_2)) it presents a sharp slope and large thinning. This crustal thinning (Moho geometry) is well established by reciprocal PmP pairs (Figures 6 G, K), that reflect from the Moho all along the profile (Figures 4C and 5C), as well as strong Pn phases (in GH, Figure 6A), that result from geometrical focusing of the energy propagating in the mantle, below the thinning region. Although tests on the internal structure of the Moho were somewhat inconclusive, they show that the crust-mantle boundary correlates with a downward velocity increase from 6.8 to 7.95 km/s. This may occur either from a very high velocity gradient across a thin layer, or abruptly across an interface. In either case, the transition from lower crust to mantle material across the Moho is always marked by a strong velocity contrast, which is required to generate the strong observed PmP (Figures Annex-1, Annex-3, and 3). Furthermore, our models can predict the presence (Figure Annex-1) or absence (Figure 3) of the Pn. These results indicate that the Moho in Domain V is still a continental Moho and therefore the lower continental crust is still present. Furthermore, while for GH the top of basement velocity decreases smoothly, for G_2H_2 the decrease of the top of basement velocity is abrupt at ~115 km in association with a deepening of ~2 km of the top of basement (Figure 9), that corresponds to ~1 s twt depicted in the MCS record section (Figure 8).

C) Domain IV (-125 – -60 km (GH); 60 – 110 km (G_2H_2)) exhibits a high velocity (6.8 – 7.25 km/s), a ~3km thick lower layer, and is the location of the disappearance of the upper continental crust, characterized by velocities ranging between 5.3 to 6.0 km/s (Figure 9). This disappearance is particularly sharp on profile G_2H_2. Since this region is located in the central part of the profile, most of the crustal phases have reciprocal phases, mainly in the lower crust (Figures 4B and 4B). Thus, the thickness, velocities, and velocity gradients are very well constrained (Figure 7), even if the crust is relatively heterogeneous (Figure Annex-4). The heterogeneity and abrupt decrease of the upper crustal velocity in Domain IVa may indicate the presence of a chaotic aggregation of collapsed blocks due to mass slump along the continental shelf. We may also speculate about a lithological contrast between a granitic and basaltic composition, yet the velocity gradient is nearly the same east and west of –115 km, which is not coherent with such hypothesis. According to Sage *et al.* (2005), this steep scarp trends N120° (Figure 1) and is controlled by a major transfer fault that crosses the Oristano Amphitheatre (Thomas *et al.*, 1988), which is formed by NNE-SSW listric normal faults and NW-SE transfer faults (Thomas *et al.*, 1988; Fais *et al.*, 1996; Lecca *et al.*, 1997). Therefore, we interpret the basement structure revealed by the velocity model as the seaward-most hanging wall of a series of tilted blocks that occurs at the foot of the slope in Domain V. Considering that in the Gulf of Lion margin Bache *et al.* (2010) identified tilted blocks in a zone of similar width, 40 – 50 km, the upper crust morphology of the conjugate pair is symmetric in Domains I and V. This zone of tilted blocks in Domain V is followed seaward by a region of partly allochthonous material in Domain IVa from large-scale mass-wasting, due to a gravitic instability associated with deep-seated faulting, that shows similar characteristics of gravitational collapse such as described in the Gulf of Biscay (Thinon *et al.*, 2003) and the Galicia margin (Clark et al., 2007). The division in the two sub-domains IVa and IVb is a consequence of the abrupt difference in thickness and velocity gradient in the upper crustal layer (Figures 9, 11B, and E). The latter is connected to a strong dome-like velocity anomaly at the base of the upper layer on profile G_2H_2. The velocity profile, featuring a clear continental Moho in Domain V, is less marked in Domain IV, where a smaller velocity contrast across the Moho is observed. An anomalous high velocity with respect to the adjacent domains characterizes the lower crust, suggesting that if lower continental crust is indeed present in Domain IV it has been transformed, since the velocity at its base has increased. Moreover, on the MCS data, the equivalent of the "T-reflector" in the Gulf of Lion is not observed at the transition between Domains V and IV, pointing to a gradual transformation of the lower continental crust inside Domain IV, instead of sharp velocity contrasts as observed in the Gulf of Lion (Moulin *et al.*, this issue). Other hypotheses can be proposed for this domain's crustal nature, namely oceanic or sub-crustal (serpentinized peridotites); however, the former does not explain the anomalous high velocity lower crust whereas the latter does not explain the velocity contrast across the Moho. We will return to this topic in the next section (see Moulin *et al.*, this issue, for more explanations).

D) Domain III is characterized by different magnetic and gravity patterns, relative to Domain IV, and interpreted as a 4km thin oceanic crust (-180 – -135 km (GH); 0 – 60 km (G_2H_2)).

1D-velocity-depth profiles and crustal nature

1D-velocity-depth profiles were extracted every 10 km (Figure 11) and compared to 1D-velocity-depth profiles of typical oceanic crust (White *et al.*, 1992) and stretched continental crust (Christensen & Mooney, 1995).

Onshore domain, Hinge Zone and Continental Slope (Domain V)

The 1D-velocity-depth profiles underneath land seismic stations (purple line on Figure 11D) show similarities with the worldwide compilation of unthinned continental crust profiles, both in velocities and gradients (Christensen & Mooney, 1995). A very small velocity step marks the transition between the upper and lower crustal layer, around a depth of 11 km.

As in the Gulf of Lion's side (see Moulin *et al.*, this issue), the 1D-velocity-depth profiles in the Hinge Zone and the continental slope domain (Figure 11A and 11D) show a similar shape but decreasing Moho depth: in each domain, the thickness decreases and the velocities slightly increase in both layers. Note that the main thinning of the upper crust occurs in the Hinge Zone (brown profiles on Figure 11D), whilst the thinning is focused mainly in the lower crust in Domain V (blue and green profiles).

Domain IV

Domain IV is the place of an important change in the 1D-velocity-depth profiles shape (light and dark orange profiles) with respect to Domain V (blue and green profiles), with a strong velocity step between the two crustal layers (more than 1 km/s) and a strong velocity gradient in the lower crust (Figures 11B and 11E). The two profiles exhibit two sub-domains with similar lower crustal layer velocities, but different upper crustal velocities: Domain IVb has an overall crustal thickness of about 5 km, whilst eastwards Domain IVa presents a thickness of 8 to 10 km, probably connected to gravity collapsed upper continental blocks over the lower layer. Neither the velocity bounds and gradients of those 1D-velocity-depth profiles, nor the thickness of Domain IVa, fit the description of typical 1D-velocity-depth profiles of oceanic crust (White *et al.*, 1992), or of stretched continental crust (Christensen & Mooney, 1995). On the other hand, Domain IVb (and Domain III), whilst thinner, exhibits 1D-velocity-depth profiles with gradients and velocities coherent with a thin oceanic crust (Figures 11C and F), therefore Domain IVb could correspond to the oldest oceanic crust emplaced during the onset of seafloor spreading. However, it is worth noting that the boundary between Domains III and IV is well marked by a drastic change in gravity and magnetic patterns, similar to the boundary between Domains II and III of the Gulf of Lion conjugate margin, where Domain II is interpreted as a thin layer of lower continental crust, exhumed along a landward deep detachment and overlying a heterogeneous, intruded layer (Moulin et al , this issue). Therefore, the potential field anomalies observed over Domain IVb are not consistent with an oceanic crust, the latter being restricted to Domain III.

Serpentinized peridotites were drilled or inferred on similar intermediate/transitional domains of northern Iberia and Newfoundland (Chian *et al.*, 1999; Dean *et al.*, 2000; Van Avendonk *et al.*, 2006). Serpentines are the result of alteration by seawater percolation through exhumed shallow mantle. The 1D-velocity-depth profiles in such areas usually have very high velocity-gradients and absence of velocity contrasts, which is very different of what it is observed on Domain IV (Figures 12 A, B, and C). Furthermore, the identification of small but clear branches of PmP phases (Figures 6I and K), requiring a velocity step at the Moho (Figure 12) which is well constrained by the critical distance of observed Pn phases (Figures Annex-2, 4C, and 5C), rules out the hypothesis of an origin of exhumed upper mantle with progressive alteration.

One could speculate that Domain IV is an exhumed part of the continental crust overlying a heterogeneous and intruded layer similar to the transitional crust of the Tagus Abyssal Plain in southwest Iberia (Afilhado *et al.*, 2008). Figure 13A presents the comparison of the 1D-velocity-depth profiles in Domains II and IV and on the Tagus Abyssal Plain. Whilst on the Gulf of Lion side the intruded lower layer (Moulin *et al.*, this issue), interpreted as a thin exhumed lower continental crust overlying a heterogeneous, fits very well with the Tagus Abyssal domain, the 1D-velocity-depth profiles of Domain IVb exhibit a very different pattern, with a much lower velocity at the top of the upper crust.

Given the large thickness of this upper layer, the very sharp transition between Domain V and IV on profile G_2H_2, and the sharp disappearance of the upper continental crust on both profiles (Figure 9), we infer that the upper layer of Domain IVa may be interpreted as fractured, gravity-collapsed continental blocks, as observed in Domain Va, in the Gulf of Biscay (Thinon *et al.*, 2003), on the Galicia margin (Clark *et al.*, 2007), and on the Gulf of Lion margin (Bache *et al.*, 2010), overlaying a thin intruded lower continental crust (Figure 10). This block seems to disappear in Domain IVb, which looks more similar to Domain III and to layer 2 of a typical oceanic crust. The dome-like velocity anomaly on Profile G_2H_2 suggests that material intruded into the upper crustal layer of Domain IVb. This strong lateral heterogeneity points to a 3D structure in the transitional domain (Figures 10 and 11), justifying the acquisition of several parallel profiles. The upper layer of that domain may therefore be stretched/intruded continental crust, basalt, or a mixture with high heterogeneity (Figure 10).

Domain III

Domain III is not well resolved everywhere in the models (Figure 7). The comparison between the 1-D velocity structure of Domain III and typical oceanic crust (White *et al.*, 1992) shows a thinner crust mainly consistent with oceanic crust (Figure 11). Nevertheless, within the data's ability to resolve the structure, Domains IVb and III show a similar overall shape in the 1D-velocity-depth profiles (Figures 11C and 11F), however they definitely present different gravity and magnetic patterns (Figure 13B). The main difference appears on Profile GH, with lower velocity and gradients in the crustal lower layer. The presence of magnetic anomalies (Figure 13B) suggests interpreting this domain as a thin oceanic crust. Nevertheless, the comparison with Domain III on the Gulf of Lion side (Figure 13C), also well marked by magnetic anomalies, shows strong differences in the 1D-velocity-depth profiles (Figure 13C): whilst in the Gulf of Lion, Domain III has a high velocity at the top of the crust (~6km/s), which can be interpreted as oceanic crust with a missing layer 2 (consisted of pillow lavas) as described in the Atlantis Bank, on the Sardinia side Domain III seems to represent a more classical but thinner oceanic crust. It is important to mention that in the last case, the velocity of the top of the basement can not reach values close to 6 km/s, since this would generate first arrivals with approximately this apparent velocity, which are not observed in either GH or G_2H_2 OBS's. Based on these observations, two hypotheses can be proposed: i) an asymmetric oceanic crust build-up, with extrusive magmatism mainly focused on the eastern side, or ii) a very heterogeneous crust in Domain III. While the latter can predict different velocities for the oceanic crust on both conjugate margins, it can not predict the affinity of the transitional and adjacent oceanic crust. The fact that the crustal basement in Domains II and IV are very similar to the adjacent atypical oceanic crust of Domain III seems to favor the first hypothesis for the conjugate pair of margins. This similarity between Domains III and IV raises the question of the role of the lower continental crust "flow", that can be gradually recrystallized to build the first atypical oceanic crust (Bott, 1971; Aslanian *et al.*, 2009; Sibuet *et al.*, 2012).

8. Conclusions

Modeling of combined wide-angle and near-vertical seismic reflection (MCS) data from two profiles along the western Sardinian margin provides, for the first time, images into the deep structure of the margin, from unthinned continental crust to oceanic crust.

Besides showing that the small scale geometry of the margin, for distances of 10 – 20 km, changes from a gentle style (GH – north profile) to a sharp style (G_2H_2 - south profile), our results also show that the large-scale trends are quite similar for both profiles. Furthermore, excluding the regions where the velocity models are poorly resolved and ill constrained, the thickness, velocity, and velocity gradient values obtained for both profiles point to similar crustal composition and a consistent evolution, defining a continental crust domain, a transitional crust domain, and an "atypical" oceanic crust domain.

The velocity at the top of the unthinned upper continental crust is ~6.0 km/s, approaching ~6.4 km/ at ~12 km depth. The lower continental crust is ~15 km thick and reaches a velocity of ~6.7 km at its base, overlaying the lithospheric mantle that has a velocity of 8.0 km/s and a vertical velocity gradient of ~0.02 km/s/km. Along the continental slope, at a distance of ~70 km, the continental crust thins to ~12 km, keeping the velocity of the lower crust unchanged. In this region, the velocity of the top of the upper continental crust decreases gently from 6.0 km/s to ~5.7 km/s, probably due to a gradual increase in fracturing, as suggested by the presence of tilted blocks with a width of 10 – 20 km. Although the thinning of the upper crust seems to be abrupt in the hinge zone for both profiles, in the lower crust it seems more gradual in the southern profile than in the northern one.

Near the foot of the continental slope, the increase of the velocity at the bottom of the crust, from ~6.7 km/s to ~7.2 km/s, is most probably related to the presence of intrusions in the lower crust. The decrease of the velocity at the top of the crust, from ~5.7 km/s to ~5.1 – 5.3 km/s, while keeping the velocity gradient approximately unchanged, is thought to be related to mass slumping and extensive fracturing of tilted fault blocks, due to gravitational slip. This process was probably more localized in the northern profile than in the southern one, still, the main point is that both profiles indicate the presence of crust with continental affinity in Domain IVa.

The change in the velocity pattern of the contiguous 30 – 40 km region (Domain IVb) encompasses an increase of the overall velocity and velocity gradient for both the upper and lower crust, as well as the last seaward deepening of the top of basement leading to a ~6 km thick crust. The upper crust velocity varies in the range of ~5.1 km/s to ~6.3 km/s while the lower crust varies in the range of ~6.7 km/s to ~7.2 km/s. This imprint is interpreted as intruded, thinned, and fractured continental crust, but it can also be related to extrusions, or most probably to both. Although the western part of the profiles is less well resolved than the central part, the transition to the adjacent thin oceanic crust is marked by an overall reduction of the crust velocity. The similarity of the upper crust velocity in Domain IV with the adjacent oceanic crust favors the presence of a basaltic cover in Domain IVb.

The two conjugate margins show an overall symmetry, although the transitional domain is shorter on the Sardinian side than on the Gulf of Lion side. Both conjugate margins show the presence of tilted blocks, in Domains I and V, followed seaward by material of continental nature in Domains II and IV. The T-reflector on the Gulf of Lion margin marks a landward deep detachment, separating the exhumed lower continental crust and a heterogeneous intruded layer of gabbros and granulites. On the Sardinia margin, the deep crust is interpreted to be intruded lower continental crust since the velocity of the deep crust varies smoothly from Domain V to IV, and no equivalent T-reflector was found. Its nature, that of an intruded or exhumed heterogeneous lower continental crust, seems similar on both sides, which does not support the hypothesis of simple shear mechanism to form the Liguro-Provencal basin.

Nevertheless, the upper crust in Domains II and IV, in the Gulf of Lion margin and Sardinia margin, respectively, differs in velocities and velocity gradients. The velocity in the transitional crust is smaller by 1 km/s in the Sardinia margin than in the equivalent Gulf of Lion margin. Similarly, the adjacent oldest oceanic crust is faster in the Gulf of Lion margin. The oldest oceanic crust displays magnetic anomalies with smaller wavelengths than the ones observed in the adjacent Domains II and IV. These two observations favor an asymmetric oceanic crust build-up, with extrusive magmatism mainly focused on the eastern side, due to the small width of the Sardinia block, the small size of Domain IV with respect to Domain II, and the presence of subduction to the east, but the hypothesis of a very heterogeneous oceanic crust cannot be ruled out. This topic will be addressed in a forthcoming paper (Aslanian *et al.*, in prep).

Acknowledgements

Many thanks also to all people involved in the SARDINIA team and crew (captain, officers, and crew of the R/V. L'Atalante), together with all people involved in the land seismic station (J.L. Olivet for Land assistance, J.P. Réhault and J. Perrot from IUEM in Sardinia, and A. Deschamp and V. Pas from Geo-Azur in Languedoc) and OBS (J. Crozon, P. Pelleau, and P. Fernagu from Ifremer, J. Begot from IUEM, E. Labahn from Geomar, and L. Allano from Bailleron) deployment. We would like also to thank the Sardinia's scientific team (L. Droz, F. Bache, J. Oudet, and E. Cosquer) who took part in the data's acquisition and contributed to the good spirit of the mission. Special thanks to EGEAC - Festas de Lisboa for the sardines.

This research was funded by Ifremer, CNRS, INSU, and the French GDR Marges-Actions-Marges program. The GMT, Zelt, and Seismic Unix software packages (Wessel & Smith, 1995; Zelt & Smith, 1992 and Cohen & Stockwell, 2003 respectively) were used to create some of the figures.

We also would like to thank the two Anonymous reviewers and editor Michel Seranne for their constructive and detailed reviews, which greatly helped improve the manuscript.

Author contributions

The Sardinia Project was imagined by J.L. Olivet and led by D. Aslanian from Ifremer. Modeling of the Sardinia-SARDE profiles was done by A. Afilhado, M. Moulin, and F. Klingelhoëfer. Processing of the deep seismic reflection data was done first by H. Nouzé and M.O. Beslier and post-stack Kirchhoff time migration by P. Schnurle. Seismic interpretations of the sedimentary sequences were done in collaboration with M. Rabineau and E. Leroux.

Figures

Figure 1 – A/ Location of the study area off the West Sardinia margin marked by the black outlined rectangle, in the general context of the Western Mediterranean Basin. The Provencal Basin was created by a counter-clockwise rotation of the Corsica–Sardinia micro-plate during the Miocene (see flowlines). The crustal Domains I to V are labeled; the « atypical » oceanic crust lying in the center of the basin (Domain III) is hatched in thin parallel black lines. The red lines indicate the location of all SARDINIA seismic profiles. GL – Gulf of Lion, PM – Provence Margin, CM – Catalan Margin, WS – West Sardinia, LS – Ligurian Sea, VT – Valencia Trough, LPB – Liguro Provencal Basin.

B/ Topographic and Bathymetric map of the study area (in meters) (modified from Berné *et al.*, 2002 & Loubrieu *et al.*, 2008), contoured every 100 m, and location of the Sardinia CROP Experiment (De Voogd *et al.*, 1991) and Riepilogo Experiment (Geletti *et al.*, 2011) seismic profiles. Main crustal domains of the margin based on seismic and magnetic analysis after Bayer et al., 1973; Galdéano &

Rossignol, 1977; Rollet *et al.*, 2002; Bache *et al.*, 2010, Oristano Amphitheatre from Thomas *et al.* (1988); Lecca *et al.* (1997) *in* Sage *et al.* (2011) and a N120° Scarp.

Figure 2 – Velocity models for the two perpendicular SARDINIA-SARDE profiles, including the model boundaries used during inversion (blue solid lines) and isovelocity contours every 0.20 km/s, OBS locations are indicated by black triangles and land seismic stations by gray triangles. Areas unconstrained by ray-tracing modeling are uncolored. Thin black lines separate the various domains. V.E.= ~4. A/ Profile G_2H_2 and B/ Profile GH.

Figure 3 – A/ Data from OBSS27 on profile G_2H_2, with the same gain, filter and scaling applied as in Fig. Annex – 1. B/ C/ and D/ Corresponding synthetic seismograms for two different hypotheses on the Moho structure in Domain Va and the Hinge Zone: B) Moho as a high velocity gradient thin layer (6.8 – 7.95 km/s in 0.2 km); C) and D) Moho as an abrupt velocity contrast across an interface (6.8 – 7.95 km/s) with C/ excluding the critical Pn; D/ including the critical Pn.

Figure 4 – A/ Upper panel: Ray coverage of the sedimentary layers of profile GH with every tenth ray from two-point ray-tracing plotting. Lower Panel: Observed travel-time picks and calculated travel-times (lines) of the sedimentary layers for all receivers along the model. B/ Same as A/ but for the crustal layers, C/ Same as A/ but for the Moho and upper mantle layers. Px stands for refracted rays from x^{th} layer, while PxP stands for reflected rays from x^{th} interface.

Figure 5 – A/ Upper panel: Ray coverage of the sedimentary layers of profile G_2H_2 with every tenth ray from two-point ray-tracing plotting. Lower Panel: Observed travel-time picks and calculated travel-times (line) of the sedimentary layers for all receivers along the model. B/ Same as A/ but for the crustal layers, C/ Same as A/ but for the Moho and upper mantle layers. Px stands for refracted rays from x^{th} layer, while PxP stands for reflected rays from x^{th} interface.

Figure 6 – Examples of ray coverage of some OBS and land seismic stations on profiles GH and G_2H_2 with observed travel-time picks and calculated travel times associated.

Figure 7 – Model resolution for all velocity nodes of the two velocity models. The same for depth nodes in the basement (squares). Gray and yellow areas can be considered well resolved. OBS positions are indicated by black triangles, land seismic stations by gray triangles. A/ Profile G_2H_2 and B/ Profile GH.

Figure 8 – Seismic reflection record sections for the two profiles. Model boundaries from wide-angle modeling converted to two-way travel-time are overlain. OBS positions are indicated by black triangles. A/ Profile G_2H_2 and B/ Profile GH.

Figure 9 – Velocity models for the two perpendicular SARDINIA-SARDE profiles including the model boundaries used during inversion (solid lines) and isovelocity contours every 0.20 km/s, OBS locations are indicated by black triangles and land seismic stations by grey triangles. Areas unconstrained by ray-tracing modeling are uncolored. Thin black lines separate the various domains. V.E.= ~4. A/ Profile G_2H_2, B/ Profile GH.

Figure 10 – Post-stack depth migration of the two profiles GH and G_2H_2, with the wide-angle reflection/refraction velocity model. Model boundaries and crustal isovelocities (at 6, 6.75, 7, and 7.25 km/s) are overlain, as well as the interpretative sketch for these profiles, based on our seismic velocity model and previous seismic interpretations.

Figure 11 – P-wave 1D-velocity-depth profiles below basement in the three distinct domains defined in this study on the profiles G_2H_2 (A, B, C) and GH (D, E, F). Each domain is compared to the compilations made for continental crust (Christensen & Mooney, 1995) and a « normal » oceanic crust (White *et al.*, 1992). 1D-velocity-depth profiles are extracted every 10 km (except in the HZ, every 5 km) in: A) the continental slope Domains Va and Vb, B) the transitional Domain IVa and IVb, C) the atypical oceanic crust domain of profile G_2H_2, D) the unthinned and the continental slope Domains HZ, Va, and Vb, E) the transitional domain IVa) and IVb, and F) the atypical oceanic crust domain of profile GH. The exact position of the extracted 1D-velocity-depth profiles is illustrated in G and H with the same colors.

Figure 12 – Comparison of 1D-velocity-depth profiles below basement profiles in Domains IVa (light orange) and IVb (orange) of Sardinia-GH (-125 – -60 km) (dotted line) and Sardinia-G_2H_2 (60 – 110 km) (full line) between the bounds of 1D-velocity-depth profiles (blue shaded areas) from wide-angle seismic models where ocean-continent transition zones was interpreted to be exhumed and/or serpentinised upper mantle: (A) CAM in the Southern Galician margin (Chian et al., 1999), (B) SCREECH line 2 in the Grand Banks margin offshore Newfoundland (Van Avendonk et al., 2006), (C) IAM-9 in Iberia Abyssal Plain (Dean *et al.*, 2000), and (D) IAM-5 wide-angle seismic model acquired at the Tagus Abyssal Plain (Afilhado *et al.*, 2008). 1D-velocity-depth profiles are extracted every 10 km on all profiles.

Figure 13 – A/ Comparison of 1D-velocity-depth below basement profiles in Domain IV (light orange lines - Sardinia-GH and Sardinia-G_2H_2), Domain II (dotted orange lines - Sardinia-AB, on the conjugate Gulf of Lion, Moulin *et al.*, this issue), and the IAM-5 wide-angle seismic model acquired at the Tagus Abyssal Plain (Afilhado *et al.*, 2008) (blue shaded area). B/ Magnetic map of the Liguro-Provencal Basin; domains are indicated by thick black lines; SARDINIA Experiment is represented by red lines. C/ The same as in A/ for Domain III (red lines - Sardinia-GH and Sardinia-G_2H_2, dotted red lines - Sardinia-AB on the conjugate Gulf of Lion, Moulin *et al.*, this issue); a « normal » oceanic crust (White *et al.*, 1992) (orange shaded envelope) is included. 1D-velocity-depth profiles are extracted every 10 km on all profiles.

Figure Annex-1 – A/ Band-pass filtered (5 – 20 Hz) seismic record section from land seismic station SRD07 on profile GH. The seismic data is gain-adjusted and time is reduced to 8 km/s, according to trace offset. B/ Synthetic seismic record section, calculated from the model for the same station using the asymptotic approach of ray theory from the Zelt code (Zelt & Ellis, 1988). The synthetic seismograms are calculated every 500 m, obtained by convolution of the impulse response with a 29-point low pass Ricker wavelet. Time and amplitude corrections according to offset are the same as in A/.

Figure Annex-2 – A/ Data from OBSS14 (oceanic domain) on profile GH, with the same gain, filter, and scaling as applied in Fig. Annex-1. B/ Corresponding synthetic seismograms.

Figure Annex-3 – A/ Data from OBSS29 (continental domain) on profile G_2H_2, with the same gain and filter applied as in Fig. Annex-1 but time reduced to 6.5 km/s. B/ Corresponding synthetic seismograms.

Figure Annex-4 - A/ Data from OBSS19 (Domain IV) on profile GH, with the same gain, filter, and scaling as applied in Fig. Annex-1. B/ Corresponding synthetic seismograms.

Table 1 – Travel-time residuals and chi-squared error for all phases and the complete model of profile GH.

Table 2 - Travel-time residuals and chi-squared error for all phases and the complete model of profile G_2H_2.

References

AFILHADO A., MATIAS L., SHIOBARA H., HIRN A., MENDES-VICTOR L. & SHIMAMURA H. (2008). - From unthinned continent to ocean: The deep structure of the West Iberia passive continental margin at 38°N. *Tectonophysics*, **458**, 9 – 50.

ANSORGE J., BLUNDELL D. & MUELLER S. (1992). Europe's lithosphere — seismic structure. *In*: D. Blundell, R. Freeman and S. Mueller (Editors), A Continent Revealed. Cambridge University Press, Cambridge, pp. 33-70.

ASLANIAN D., MOULIN M., OLIVET J-L., UNTERNEHR P., BACHE F., RABINEAU M., MATIAS L., NOUZÉ H., KLINGELHOEFER F., CONTRUCCI I. & LABAILS C. (2009). Brazilian and African passive margins of the Central Segment of the South Atlantic Ocean: kinematic constraints, *Tectonophysics*, **468**, 98-112.

AYALA C., POUS J. & TORNÉ M. (1996). The lithosphere-astenosphere boundary of the Valencia trough Western Mediterranean/deduced from 2D geoid and gravity modelling. *Geophysical Research Letters*, 23, **22**, 3131 – 3134.

AUFFRET Y., PELLEAU P., KLINGELHOEFER F., GÉLI L., CROZON J., LIN J.I. & SIBUET J.-C. (2004). MicrOBS : a new generation of bottom seismometer, *First Break*, **22**, 41-47.

AUZENDE J.M., BONNIN J. & OLIVET J.L. (1973). The origin of the Western Mediterranean basin, *J. Geol. Soc. Lond.*, **19**, 607–620.

AVEDIK F., RENARD V., ALLENOU J. & MORVAN B. (1993). Single bubble air-gun array for deep exploration, *Geophysics*, **58**, 366–382.

BACHE F., OLIVET J.-L., GORINI C., RABINEAU M., BAZTAN J., ASLANIAN D. & SUC J.-P. (2009). Messinian erosional and salinity crises: View from the Provence Basin (Gulf of Lions, Western Mediterranean), *Earth and Planetary Science Letters*, **286**, 139–157.

BACHE F., OLIVET J.-L., GORINI C., ASLANIAN D., LABAILS C. & RABINEAU M. (2010). Evolution of rifted continental margins: The case of the Gulf of Lions (Western Mediterranean Basin), *Earth and Planetary Science Letters*, **292**, 345-356.

BAYER R., LE MOUEL J.L. & LE PICHON X. (1973). Magnetic anomaly pattern in the western Mediterranean. *Earth and Planetary Science Letters*, **19** (2), 168-176.

BERNÉ S., ALOÏSI J.C., BAZTAN J., DENNIELOU B., DROZ L., DOS REIS T., LOFI J., MÉAR Y. & RABINEAU M. (2002). Notice de la carte morphobathymétrique du Golfe du Lion, Brest, IFREMER et Région Languedoc Roussillon 1, 48.

BIJU DUVAL B. & MONTADERT, L. (1977). Introduction to the structural history of the Mediterranean Basins. In: Int. Symp. Struct. Hist. Medit. Basins, Split, 1976. Technip, Paris, pp. 1-12.

BOCCALETTI, M. & GUAZZONE, G. (1974). Remnant arcs and marginal basins in the Cainozoic development of the Mediterranean. *Nature*, **252**, 18-21.

BOTT, M.H.P. (1971). Evolution of young continental margins and formation of shelf basin. *Tectonophysics*, **11**, 319-37.

BRUN J.P. & BESLIER M.O. (1996). Mantle exhumation at passive margins. *Earth and Planetary Science Letters*, **142**, 161-173.

CARBONELL R., LEVANDER A., & KIND R. (2013). The Mohoroviçi discontinuity beneath the continental crust: An overview of seismic constraints, *Tectonophysics*, **609**, 353–376.

CARMIGNANI L., CAROSI R., DI PISA A., GATTIGLIO M., MUSUMECI G., OGGIANO G. & PERTUSATI P.C. (1994). The Hercynian chain in Sardinia (Italy). *Geodinamica Acta*, **7**, 31–47

CARMINATI E., DOGLIONI C., GELABERT B., PANZA G.F., RAYKOVA R.B., ROCA E., SABAT F. & SCROCCA D. (2012). Evolution of the Western Mediterranean, in Phanerozoic Passive Margins, Cratonic Basins and Global Tectonic Map (David G. Roberts, A.W. Bally: eds). Doi10.1016/B978.0.444.56357.6.00011.1

CASSANO E., MARCELLO A., NANNINI R., PRETTI S., RANIERI G., SALVADERI R. & SALVADORI I. (1979). Rilievo aeromagnetico della Sardegna e de1 mare circostante. In: Ente Minerario Sardo, **3**, l-30.

CASSANO E. (1990). Tyrrhenian and Western Mediterranean geomagnetic domains. *Terra-nova*, **2**, 638-644.

CHAMOT-ROOKE N., JESTIN F. & GAULIER J. (1999). Constraints on Moho depth and crustal thickness in the Liguro-Provencal Basin from 3D gravity inversion: geodynamic implications. In: The Mediterranean Basins: Tertiary extension within the Alpine Orogen (B. Durand, L. Jolivet, F. Horvath and M. Séranne (Eds)), *Geol. Soc. of London, Special Publication*. **156**, 37-61.

CHIAN D.P., LOUDEN K.E., MINSHULL T.A. & WHITMARSH R.B. (1999). Deep structure of the ocean–continent transition in the southern Iberia Abyssal Plain from seismic refraction profiles: Ocean Drilling Program (Legs 149 and 173) transect. *Journal of Geophysical Research-Solid Earth*, **104**, 7443–7462.

CHRISTENSEN N. & MOONEY W. (1995). Seismic velocity structure and composition of the continental crust: a global view. *Journal of Geophysical Research*, **100**, (B6) doi:10.1029/95JB00259.

CITA M.B. & GARTNER S. (1973). Studi sul Pliocene e uli strati di passaggio dal Miocene al Pliocene IV. The stratotype Zanclean foraminiferal and nannofossil biostratigraphy. *Riv. Ital. Paleont.*, **79** (4), 503–558.

CLARK S.A., SAWYER D.S., AUSTIN J.A. JR., CHRISTESON G.L. & NAKAMURA Y. (2007). Characterizing the Galicia Bank-Southern Iberia Abyssal Plain rifted margin segment boundary using multichannel seismic and ocean bottom seismometer data, *Journal of Geophysical Research-Solid Earth*, **112**, B03408, doi:10.1029/2006JB004581.

CLAUZON G. (1978). The Messinian Var canyon (Provence, Southern France) — paleogeographic implications. *Marine Geology*, **27**, 231–246.

CLOETINGH S., BUROV E., MATENCO L., BEEKMAN F., ROURE F. & ZIEGLER P.A. (2013). The Moho in extensional tectonic settings: Insights from thermo-mechanical models, *Tectonophysics*, **609**, 558–604.

COHEN J. K. & STOCKWELL JR J. W. (2000). CPW/SU: Seismic Unix Release 34, a free package for research and processing. *Center for Wave Phenomena, Colorado School of Mines*.

COLLIER J.S., BUHL P., TORNE M. & WATTS A.B. (1994). Moho and lower crustal reflectivity beneath a young rift basin/results from a two-ship, wide aperture seismic reflection experiment in the Valencia Trough (western Mediterranean). *Geophysical Journal International*, **118**, 159–180.

CONTRUCCI I., NERCESSIAN A., BÉTHOUX N., MAUFFRET A. & PASCAL G. (2001). A Ligurian (Western Mediterranean Sea) geophysical transect revisited. *Geophysical Journal International*, **146**, 74-97.

CORNÉE J.J., MAILLARD A., CONESA G., GARCÍA F., SAINT MARTIN J.P., SAGE F. & MÜNCH P. (2008). Onshore to offshore reconstruction of the Messinian erosion surface in western Sardinia, Italy: MSC implications. *Sedimentary Geology*, **210** (1–2), 48–60.

CURZI P., ROSSI P.L. & SARTORI R. (1982). Dati geologici e petrografici sul basamento della scarpata occidentale della Sardegna. G. *Geol.*, **2**, 45(l): 1-15.

DEAN S.M., MINSHULL, T.A. WHITMARSH R.B. & LOUDEN K.E. (2000). Deep structure of the ocean–continent transition in the southern Iberia Abyssal Plain from seismic refraction profiles: The IAM-9 transect at 40 degrees 20 ' N. *Journal of Geophysical Research-Solid Earth*, **105** (B3), 5859–5885.

DE VOOGD B., NICOLICH R., OLIVET J.L., FANUCCI F., BURRUS J., MAUFFRET A., PASCAL G., ARGNANI A., AUZENDE J.M., BERNABINI M., BOIS C., CARMIGNANI L., FABBRI A., FINETTI I., GALDEANO A., GORINI C.Y., LABAUME P., LAJAT D., PATRIAT P., PINET B., RAVAT J., RICCI LUCHI F. & VERNASSA S. (1991). First deep seismic reflection transect from the Gulf of Lions to Sardinia (ECORS–CROP profiles in Western Mediterranean), *In*: Meissner, R., Brown, L., Durbaum, H.-J., Fuchs, K., Seifert, F. (Eds.), Continental Lithosphere: Deep Seismic Reflections. v. Geodynamics, **22**. *American Geophysical Union*, Washington, pp. 265–274.

DOS REIS A.T., GORINI C. & MAUFFRET A. (2005). Implications of salt–sediment interactions on the architecture of the Gulf of Lions deep-water sedimentary systems—western Mediterranean Sea, *Marine and Petroleum Geology*, **22**, 713–746.

FAIS S., KLINGELE E. E. & LECCA L. (1996). Oligo-Miocene half graben structure in Western Sardinian Shelf (western Mediterranean): reflection seismic and aeromagnetic data comparison. *Marine geology*, **133**(3), 203-222.

FANUCCI F., FIERRO G., ULZEGA A., GENNESSEAUX M., REHAULT J.P. & VIARIS DE LESEGNO L. (1976). The continental shelf of Sardinia: structure and sedimentary characteristics. *Boll. Sot. Geol. Ital.*, **95**, 1207-1217.

FINETTI I. & MORELLI C. (1973). Esplorazione geofisica dell'area circostante il blocco sardo-torso. *Rend. Sem. Fat. Sci. Univ. Cagliari*, Suppl., 43: 213-238.

GAILLER A., KLINGELHOEFER F., OLIVET J.-L., ASLANIAN D. & THE SARDINIA SCIENTIFIC AND TECHNICAL OBS TEAMS (2009). Crustal structure of a young margin pair: New results across the Liguro–Provencal Basin from wide-angle seismic tomography, *Earth and Planetary Science Letters*, **286**, 333-345.

GALSON D. A. & MUELLER S. (1987). The European Geotraverse (EGT) Project: A Progress Report. Amer. Geophys. Union, Geodynamics Series, vol. 16, p. 253-272.

GALDEANO A. & ROSSIGNOL J. C. (1977). Assemblage à altitude constante des cartes d'anomalies magnétiques couvrant l'ensemble du bassin occidental de la Méditerranée. *Bulletin de la Société géologique de France*, **3**, 461-468.

GELETTI R., ZGUR F., DEL BEN A., BURIOLA F., FAIS S., FEDI M., FORTE E., MOCNIK A., PAOLETTI V., PIPAN M. RAMELLA R., ROMEO & ROMI A. (2014). West-Sardinian Margin and Eastern Balearic basin (West Mediterranean Sea) : evidence of regional geological features, *Marine Geology*, **351**, 76-90.

GELETTI R., ZGUR F., DEL BEN A., FAIS S., FEDI M., FORTE E., MOCNIK A., PIPAN M., ROMEO R., TOMINI I. & RAMELLA R. (2011). Geophysical Study of the W-Sardinia Margin. GNGTS.

GORINI C., LE MARREC A. & MAUFFRET A. (1993). Contribution to the structural and sedimentary history of the Gulf of Lions (Western Mediterranean) from the ECORS profiles, industrial seismic profiles and well data. *Bull. Soc. géol. Fr.*, **164**, 353–363.

GUENNOC P., GORINI C. & MAUFFRET A. (2000). Histoire géologique du Golfe du Lion et cartographie du rift oligo-aquitanien et de la surface messinienne. *Géol. Fr.*, **3**, 67–97.

HUISMANS R.S. & BEAUMONT C. (2008). Complex rifted continental margins explained by dynamical models of depth-dependent lithospheric extension. *Geology*, **36**, 163-166.

HUISMANS R.S. & BEAUMONT C. (2011). Depth-dependent extension, two-stage breakup and cratonic underplating at rifted margins, *Nature*, **473**, 74-78, doi:10.1038/nature09988.

HSÜ K.J., CITA M.B. & RYAN W.B.F. (1973). The origin of the Mediterranean evaporites. In: Leg 13 (Ed. by W.B.F. Ryan & K.J. Hsü et al.), *Init. Rep. Deep Sea Drill. Proj.*, **13**, 1203–1231.

JOLIVET L. & FACCENNA C. (2000). Mediterranean extension and the Africa–Eurasia collision. *Tectonics*, **19**, 1095–1106.

JOLIVET L. R., AUGIER C., ROBIN J. P., SUC & ROUCHY J. M. (2006). Lithospheric-scale geodynamic context of the Messinian Salinity Crisis. *Sediment. Geol.*, **188**, 9-33.

KUSZNIR N.J. & KARNER G. D. (2007). Continental lithospheric thinning and breakup in response to upwelling divergent mantle flow: applcation to the Woodlark, Newfounland and Iberia margins, *In: Karner, G. D., Manatschal, G. & Pinherio, L. M. (eds), Imaging, Mapping and Modelling Continental Lithosphere Extension and Breakup, Geological Society, London, Special Publications*, **282**, 389-419.

LAVIER L. & MANATSCHAL G. (2006). A mechanism to thin the continental lithosphere at magma-poor margins, *Nature*, **440**, 324-328, doi:10.1038/nature04608.

LE DOUARAN S., BURRUS J. & AVEDIK F. (1984). Deep structure of the North-Western Mediterranean basin: results of a two-ship seismic survey, *Marine Geology*, **55**, 325–345.

LE PICHON X., PAUTOT G., AUZENDE J. & OLIVET J. (1971). La méditerranée occidentale depuis l'oligocene : schema d'évolution. *Earth and Planetary Science Letters*, **13**, 145-152.

LECCA L. (1982). La piattaforma continentale della Sardegna occidentale. Nota preliminare. *Rend. Sot. Geol. Ital.*, 5:93-97.

LECCA L., CARBONI S., SCARTEDU R. F., TILOCCA G. & PISANO S. (1986). Schema stratigrafico della piattaforma continentale occidentale e meridionale della Sardegna. *Mem. Sot. Geol. Ital.*, **36**: 31-40.

LECCA L., LONIS R., LUXORO S., MELIS E., SECCHI F. & BROTZU P. (1997). Oligo-Miocene volcanic sequences and rifting stages in Sardinia : a review. Periodico di Mineralogi, 66, 7-61.

LOFI J., RABINEAU M., GORINI C., BERNE S., CLAUZON G., DE CLARENS P., DOS REIS A.T., MOUNTAIN G.S., RYAN W.B.F., STECKLER M.S. & FOUCHET C. (2003). Plio-Quaternary prograding clinoform wedges of the western Gulf of Lion continental margin (NW Mediterranean) after the Messinian Salinity Crisis. *Marine Geology*, **198**, 289-317.

LOFI J., DEVERCHÈRE J., GAULLIER V., GILLET H., GORINI C., GUENNOC P., LONCKE L., MAILLARD A., SAGE F. & THINON I. (2011). Seismic Atlas of the Messinian Salinity Crisis markers in the Mediterranean and Black Seas. Commission for the Geological Map of the World. Memoires de la Société Géologique de France, n.s., 179, 72p, 1CD.

LOUBRIEU B., MASCLE J. & THE CIESM / IFREMER MEDIMAP GROUP (2008). Morpho-bathymetry of the Mediterranean Sea, CIESM edition.

MALINVERNO A. & RYAN W.B.F. (1986). Extension in the Tyrrhenian Sea and shortening in the Apennines as a result of arc migration driven by the sinking of the lithosphere. *Tectonics*, **5**, 227–245.

MAILLARD A. & MAUFFRET A. (1999). Crustal structure and riftogenesis of the Valencia Trough (north-western Mediterranean Sea). *Basin Research*, **11**(4), 357–379.

MAUFFRET A., MAILLARD A., PASCAL G., TORNE M., BUHL P. & PINET B. (1992). Long-listening Multichannel Seismic Profiles in the Valencia Trough (Valsis 2) and the Gulf of Lion (ECORS): a comparison. *Tectonophysis*, **203**, 285-304.

MAUFFRET A., PASCAL G., MAILLARD A. & GORINI C. (1995). Tectonics and deep structure of the north-western Mediterranean Basin. *Marine and Petroleum Geology*, **12**, 645-666.

MJELDE R., GONCHAROV A. & MÜLLER R.D. (2013). The Moho: Boundary above upper mantle peridotites or lower crustal eclogites? A global review and new interpretations for passive margins, *Tectonophysics,* **609,** 636–650.

MOULIN M., KLINGELHOEFER F., AFILHADO A., ASLANIAN D., SCHNURLE P., NOUZÉ H., RABINEAU M., BESLIER M.O. & FELD A. (in press). Deep crustal structure across a young passive margin from wide-angle and reflection seismic data (The SARDINIA Experiment) - I. Gulf of Lion's margin. *Bulletin de la Société géologique de France,* this issue.

MULLER M. R., ROBINSON C. J., MINSHULL T. A., WHITE R. S. & BICKLE M. J. (1997). Thin crust beneath ocean drilling program borehole 735B at the Southwest Indian Ridge?. *Earth and Planetary Science Letters*, **148**(1), 93-107.

MUTTER J.C. & CARTON H.D. (2013). The Mohorovicic discontinuity in ocean basins: Some observations from seismic data, *Tectonophysics*, **609**, 314–330.

NIELSEN, C., & THYBO H. (2009). Lower crustal intrusions beneath the southern Baikal Rift Zone: Evidence from full-waveform modelling of wide-angle seismic data, *Tectonophysics*, **470**, 298 – 318, doi:10.1016/j.tecto.2009.01.023.

PASCAL G.P., MAUFFRET A. & PATRIAT P. (1993). The ocean–continent boundary in the Gulf of Lion from analysis of expanding spread profiles and gravity modelling, *Geophysical Journal International*, **113**, 701–726.

RÉHAULT J.-P., BOILLOT G. & MAUFFRET A. (1984). The western Mediterranean Basin geological evolution. *Marine Geology*, **55**, 447-477.

ROLLET N., DÉVERCHÈRE J., BESLIER M.-O., GUENNOC P. RÉHAULT J.-P., SOSSON M. & TRUFFERT C. (2002). Back arc extension, tectonic inheritance and volcanism in the Ligurian Sea, western Mediterranean. *Tectonics*, **21**, doi: 10.1029/2001TC900027.

RYAN W.B.F., HSU K.J., CITA M.B., DUMITRICA P., LORT J.M. MAYNC W., NESTEROFF W.D., PAUTOT G., SATARDNER H. & WESES F.C. (1973). Boundary of Sardinia Slope with Balearic abyssal plain-sites 133 and 134. In: W.B.F. Ryan, K.J. Hsii et al., Init. Rep. DSDP, 13: 465-514.

RYAN W. F. B. (1976). Quantitative evaluation of the depth of the Western Mediterranean before, during and after the Messinian salinity crisis. *Sedimentology*, **23**, 791-813.

SABAT F., ROCA E., MUNOZ J.A., VERGÉS J., SANTANACH P., SANS M., MASANA E., ESTÉVEZ A. & SANTISTEBAN C. (1997). Extension and compression in the evolution of the eastern margin off Iberia: the ESCI-Valencia Trough seismic profile. *Rev. Soc. Geol. Espana*, **8** (4), 431-448.

SAGE F., DEVERCHÈRE J., VON GRONEFELD G., GAULLIER V., GORINI C., MAILLARD A. & CORNÉE J.-J. (2011). Western Sardinia, chapt. 8 in Seismic Atlas of the Messinian Salinity Crisis markers in the Mediterranean and Black Seas of Lofi et al., 2011.

SAGE F., VON GRONEFELD G., DEVERCHÈRE J., GAULLIER V., MAILLARD A. & GORINI C. (2005). Seismic evidence for Messinian detrital deposits at the western Sardinia Margin, northwestern Mediterranean. *Marine and Petroleum Geology*, **22**, 757-773.

SÉRANNE M. (1999). The gulf of Lion continental margin (NW Mediterranean) revisited by IBS: an overview. In Durand, B., Jolivet, L., Horvath, F & Séranne M., (Eds), The Mediterranean Basins: Tertiary Extension Within the Alpine Orogen. *Geol. Soc. of London, Special Publication*, **156**, 15-36.

SÉRANNE M., BENEDICTO A., TRUFFERT C., PASCAL G. & LABAUME P. (1995). Structural style and evolution of the Gulf of lion Oligo-Miocene rifting, Role of the Pyrenean orogeny. Marine and Petroleum Geology, **12**, 809–820.

SIBUET J.C. & TUCHOLKE, B. (2012). The geodynamic province of transitional lithosphere adjacent to magma-poor continental province. *In* Mohriak, W. U., Danforth, A., Post, P. J., Brown, D. E., Tari, G. C., Nemcˇok, M.&Sinha, S. T. (eds), Conjugate Divergent Margins. *Geological Society, London,* Special Publications, 369, http://dx.doi.org/10.1144/SP369.15

THOMAS B., LECCA L. & GENNESSEAUX M. (1988). Structuration et morphogénèse de la marge occidentale de la Sardaigne au Cénozoique. *Compte Rendu de l'Académie des Sciences*, **306**, 903-910.

TORNÉ M., PASCAL G., BUHL P., WATTS A.B. & MAUFFRET A. (1992). Crustal and velocity structure of the Valencia trough (western Mediterranean), Part I. A combined refraction/ wide-angle reflection and near-vertical reflection study, *Tectonophysics*, **203**, 203,1-20.

THINON L ., MATIAS L., RÉHAULT J.P., HIRN A., FIDALGO-GONZÁLEZ L. & AVEDIK F. (2003). Deep structure of the Armorican Basin (Bay of Biscay): a review of Norgasis seismic reflection and refraction data, *Journal of the Geological Society*, London, **160**, 99–116.

THYBO H. & ARTEMIEVA I.M. (2013). Moho and magmatic underplating in continental lithosphere, *Tectonophysics,* **609**, 605–619.

VAN AVENDONK H. J., HOLBROOK W. S., NUNES G. T., SHILLINGTON D. J., TUCHOLKE B. E., LOUDEN K. E., LARSEN H.C. & HOPPER J. R. (2006). Seismic velocity structure of the rifted margin of the eastern Grand Banks of Newfoundland, Canada. *Journal of Geophysical Research: Solid Earth*, **111**(B11), 1978–2012.

WATREMEZ L., LEROY S., ROUZO S., D'ACREMONT E., UNTERNEHR P., EBINGER C., LUCAZEAU F. & AL-LAZKI A. (2011). The crustal structure of the north-eastern Gulf of Aden continental margin: insights from wide-angle seismic data, *Geophysical Journal International*, **184**, pp. 575–594.

WATTS A.B., TORNE M., BUHL P., MAUFFRET A., PASCAL G. & PINET B. (1990). Evidence for reflectors in the lower continental crust before rifting in the Valencia Trough. *Nature*, **348**, 631-634.

WESSEL P. & SMITH W. H. (1998). New, improved version of Generic Mapping Tools released. *Eos, Transactions American Geophysical Union*, **79**(47), 579-579.

WHITE R. S., MCKENZIE D. & O'NIONS R. (1992). Oceanic crustal thickness from seismic measurements and rare earth element inversions. *J. Geophys. Res.*, **97**, 19,683-19,715.

ZELT C.A. & ELLIS R.M. (1988). Practical and efficient ray tracing in two-dimensional media for rapid traveltime and amplitude forward modelling. *Canadian Journal of Exploration Geophysics*, **24**, 16–31.

ZELT C.A. & SMITH R.B. (1992). Seismic travel time inversion for 2-D crustal velocity structure, *Geophysical Journal International*, **108**, 16–34.

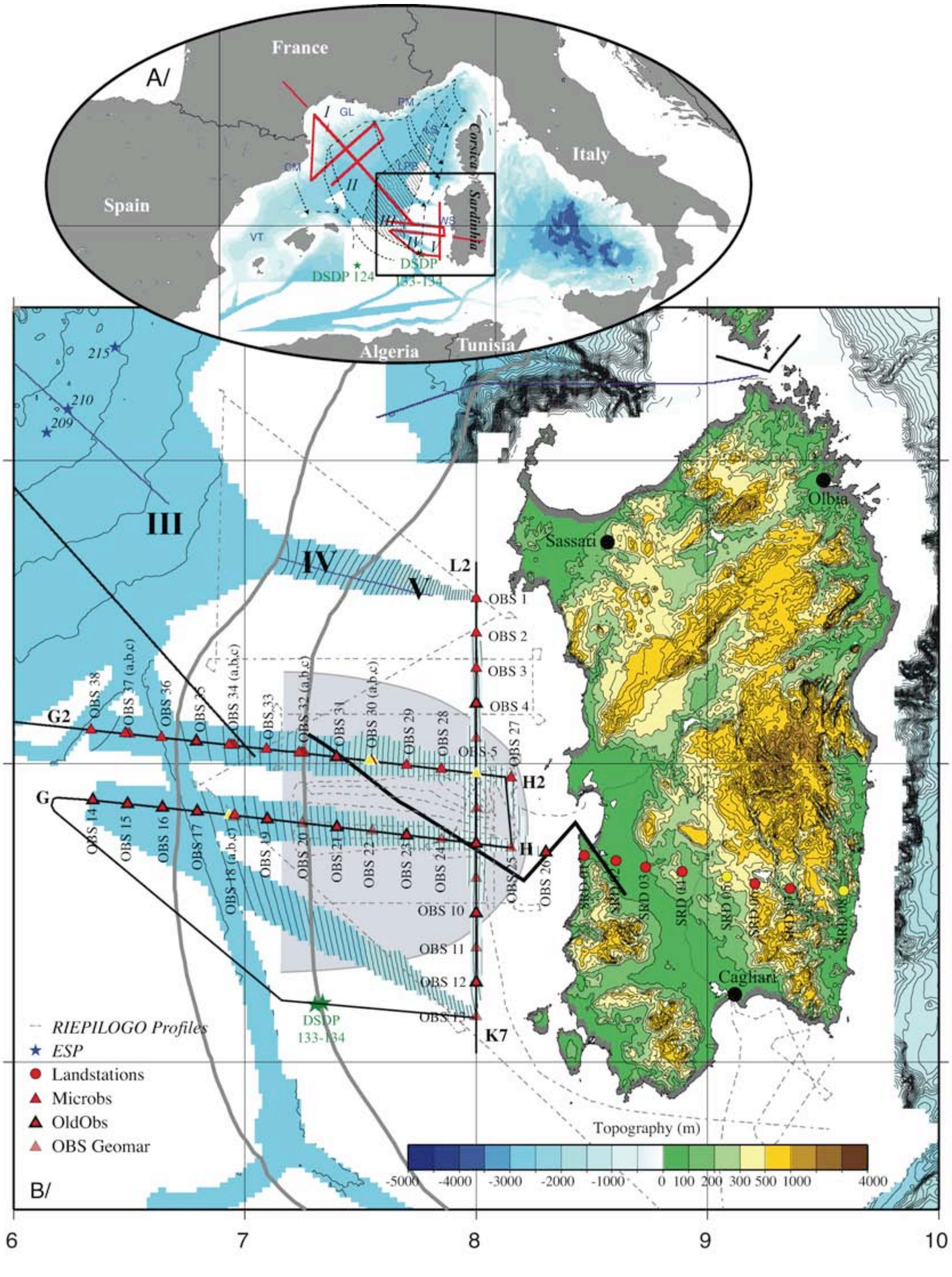

1019 **Figure 1** - Sardinia SARDE

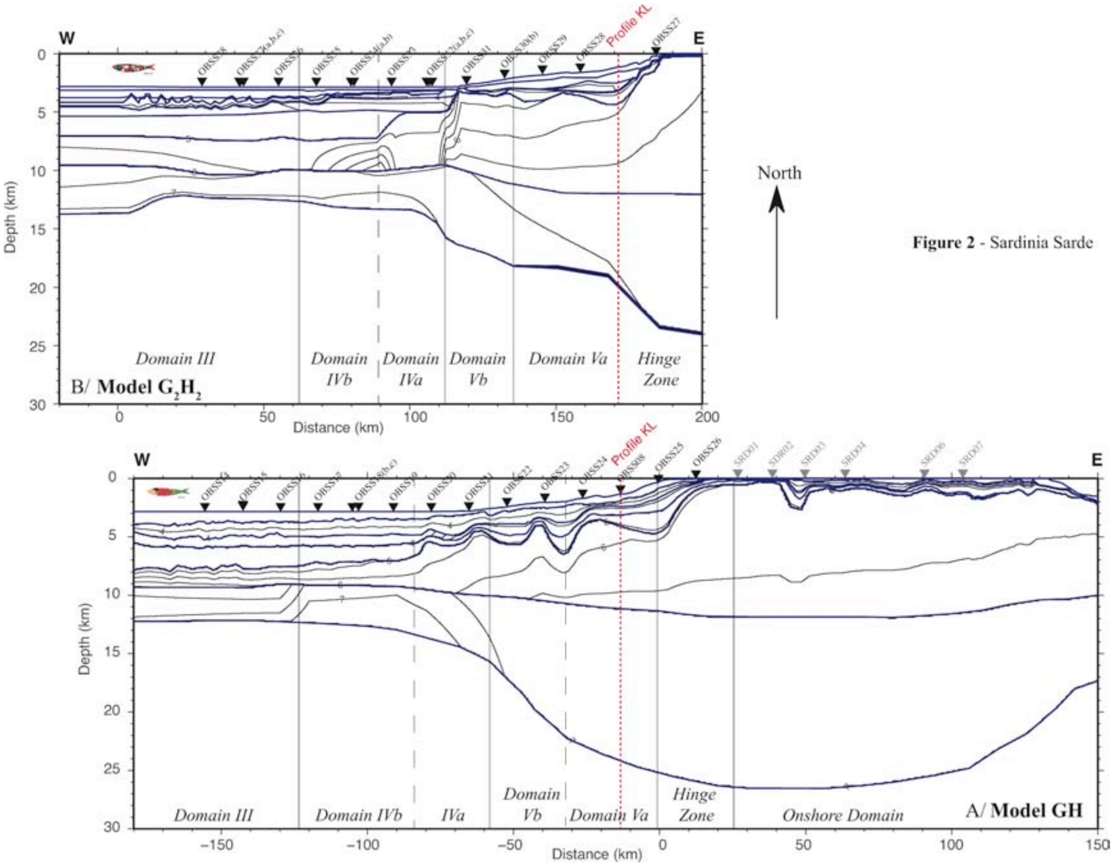

Figure 2 - Sardinia Sarde

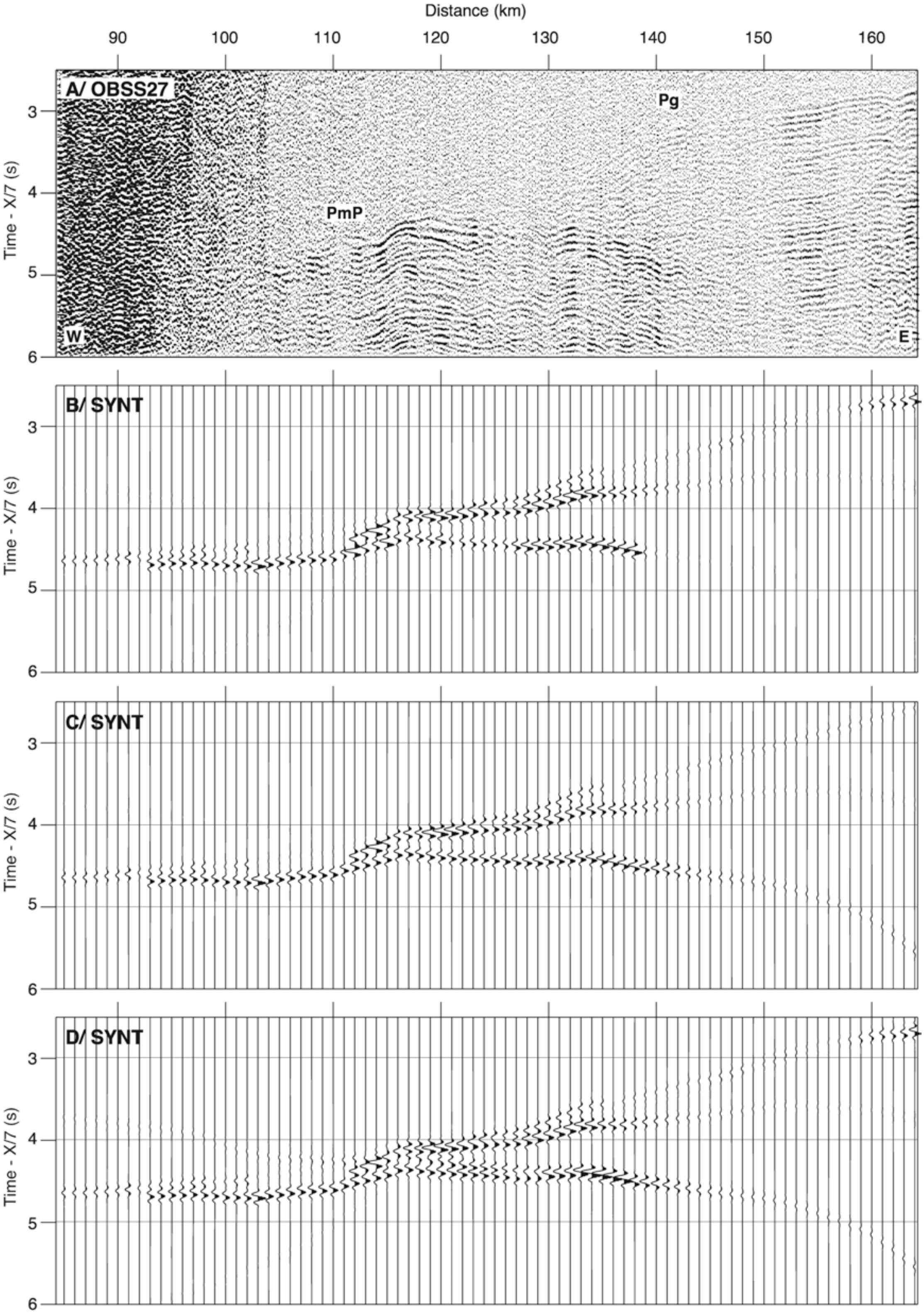

Figure 3 - Sardinia SARDE

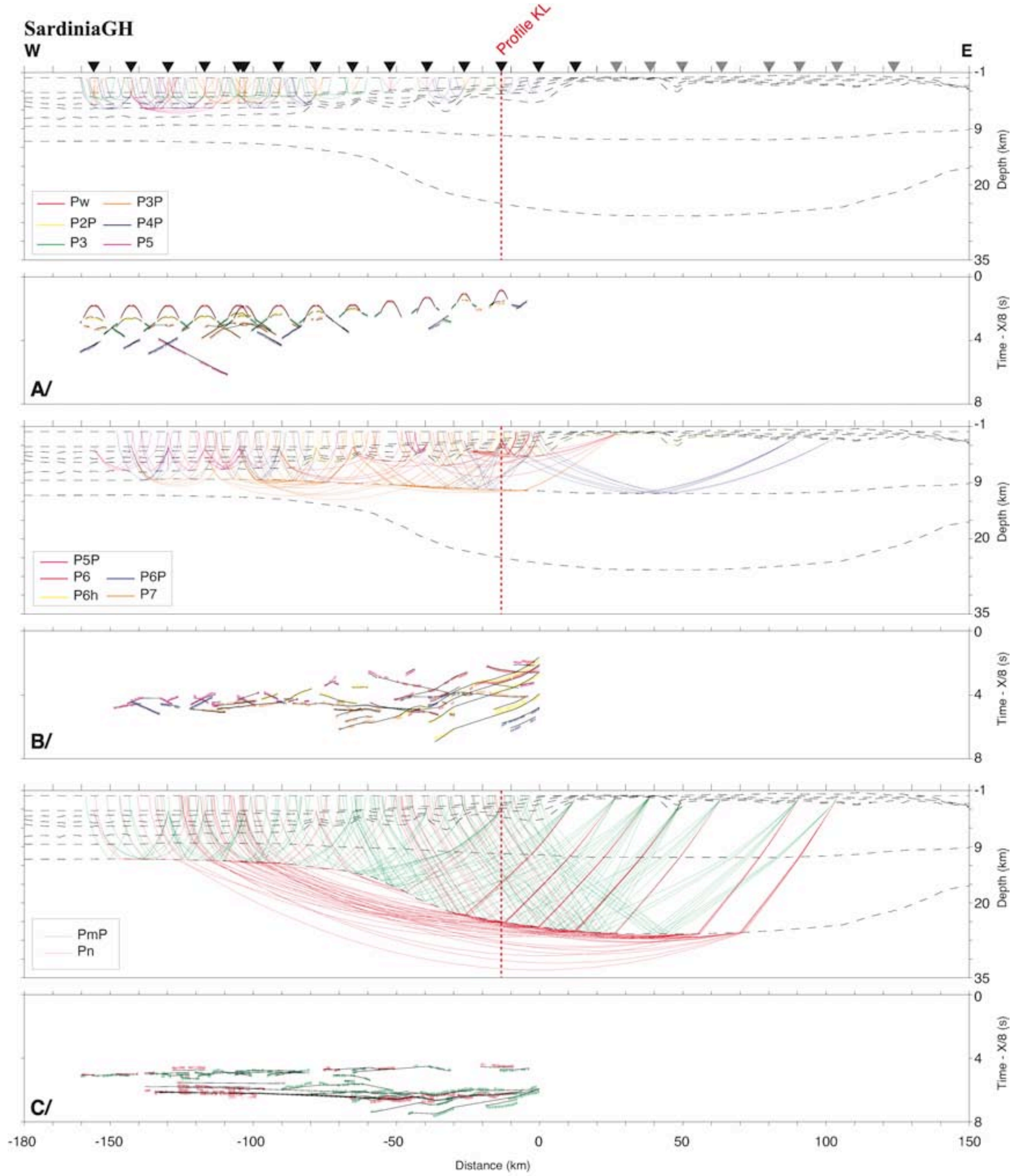

1022 **Figure 4** - Sardinia Sarde

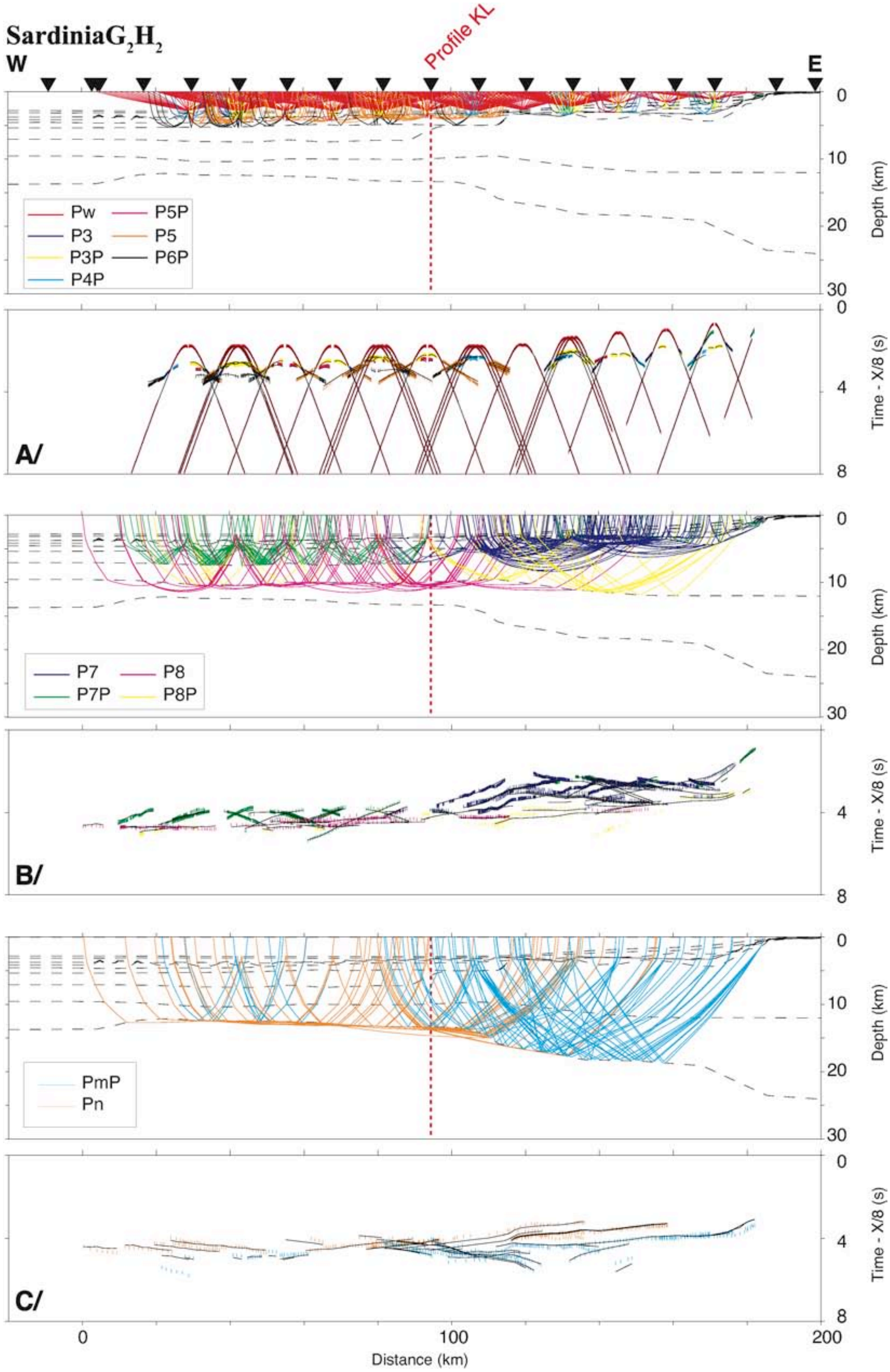

1023 **Figure 5** - Sardinia Sarde

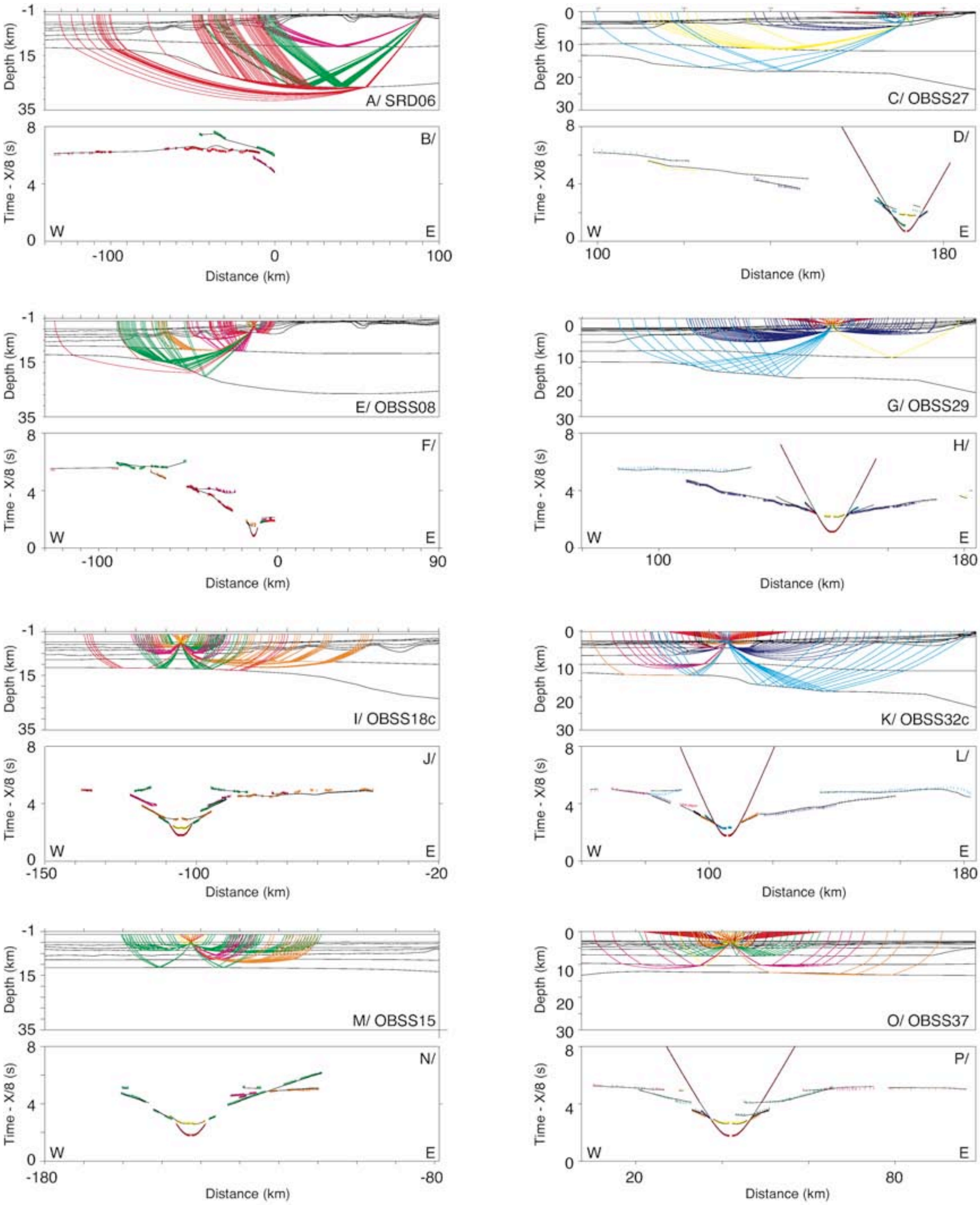

1024 **Figure 6** - Sardinia Sarde

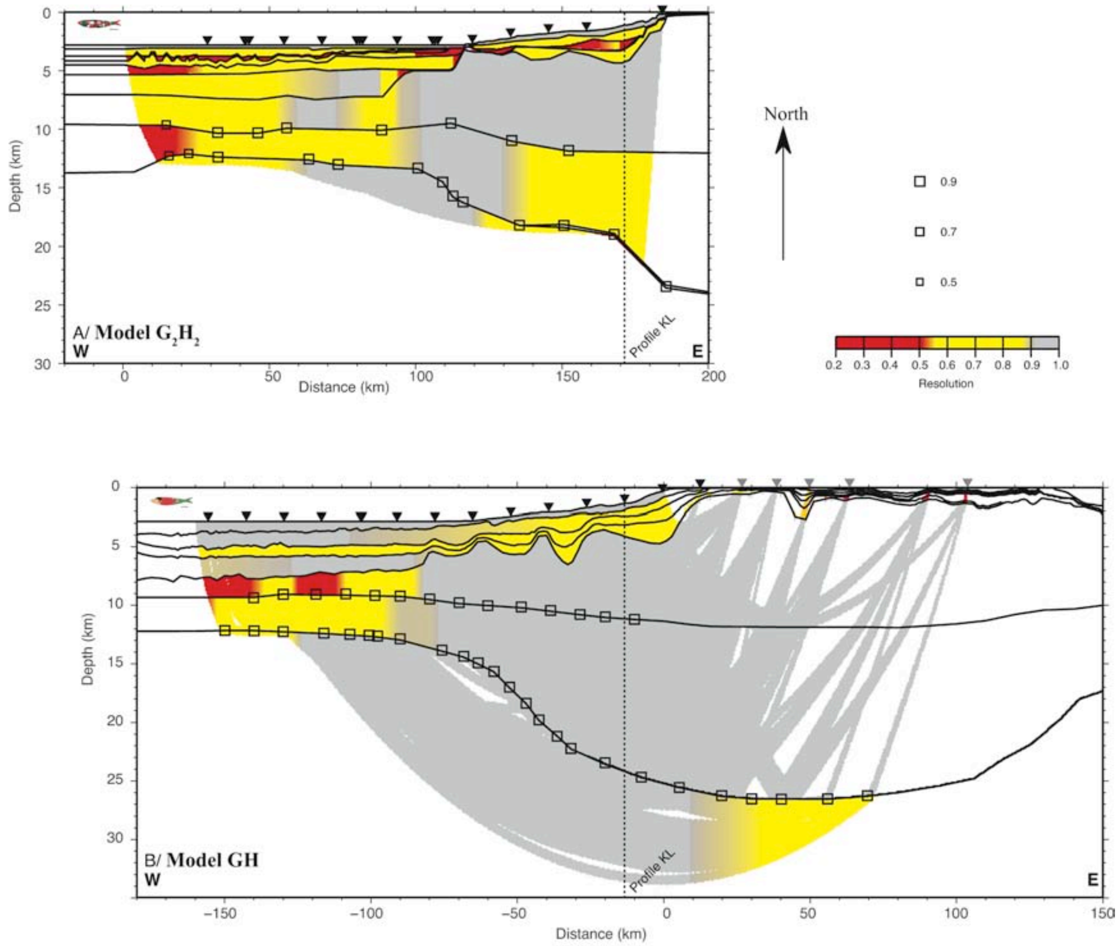

Figure 7 - Sardinia Sarde

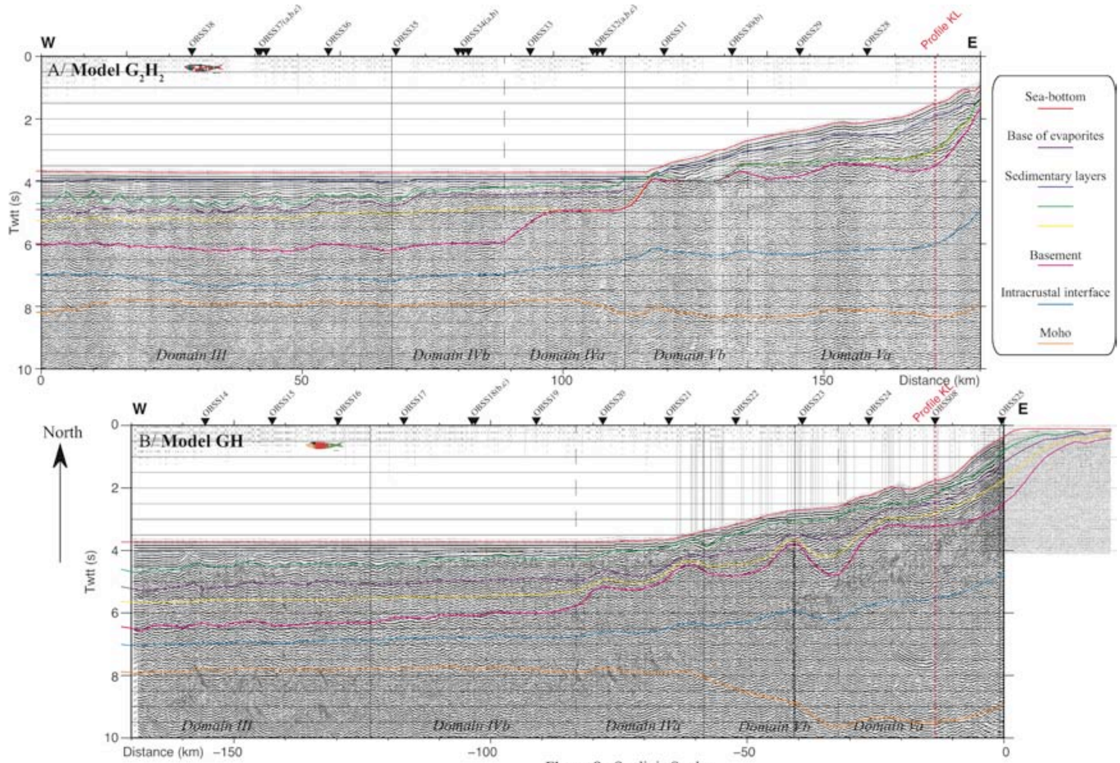

Figure 8 - Sardinia Sarde

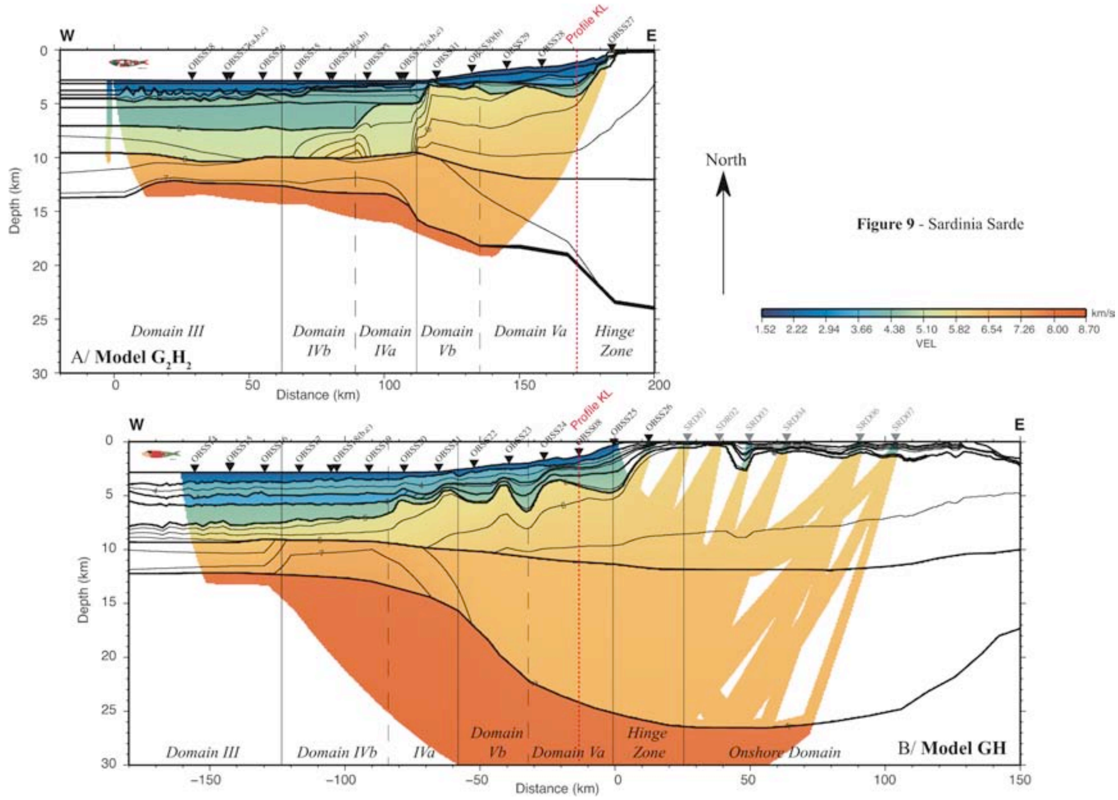

Figure 9 - Sardinia Sarde

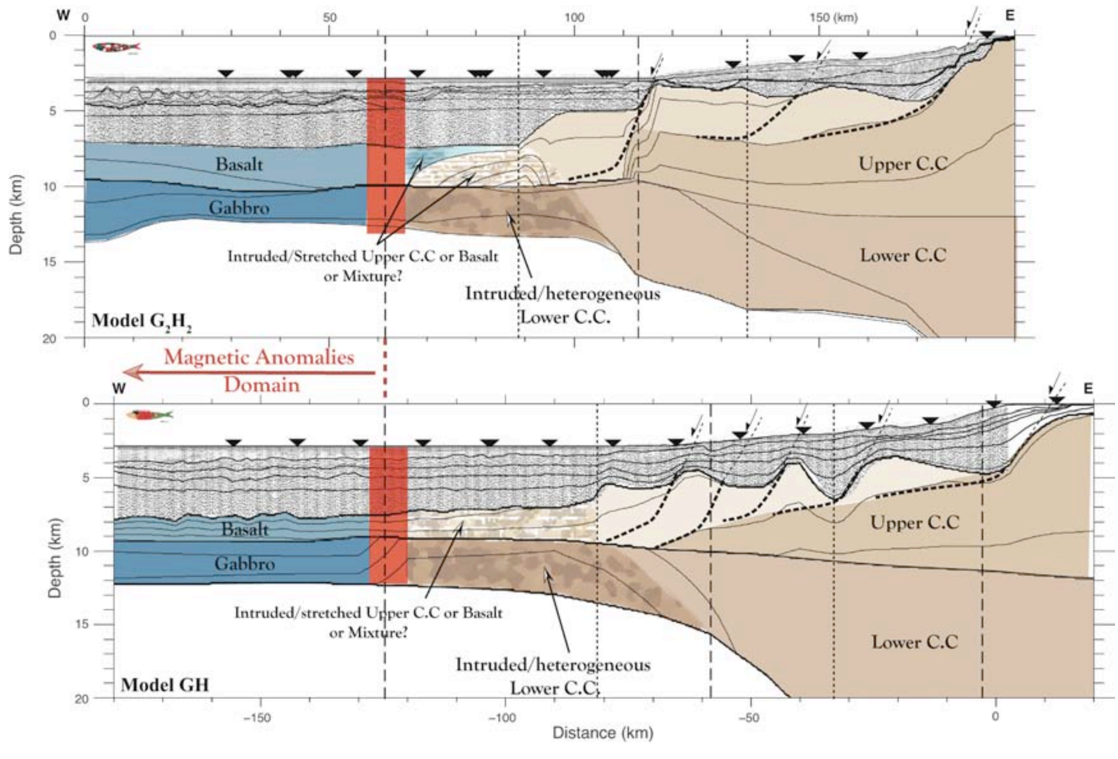

Figure 10 - Sardinia Sarde

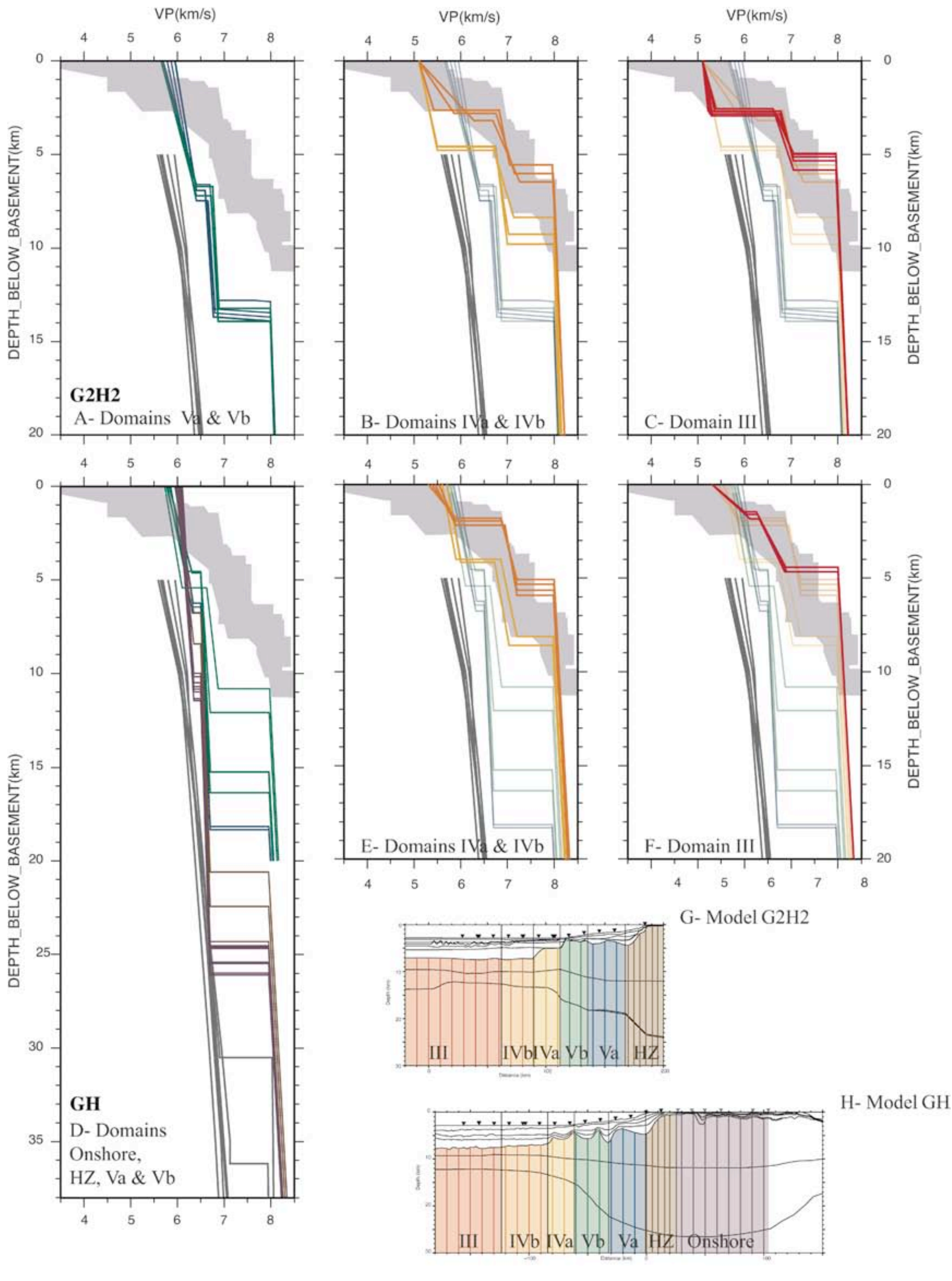

1029 **Figure 11** - Sardinia Sarde

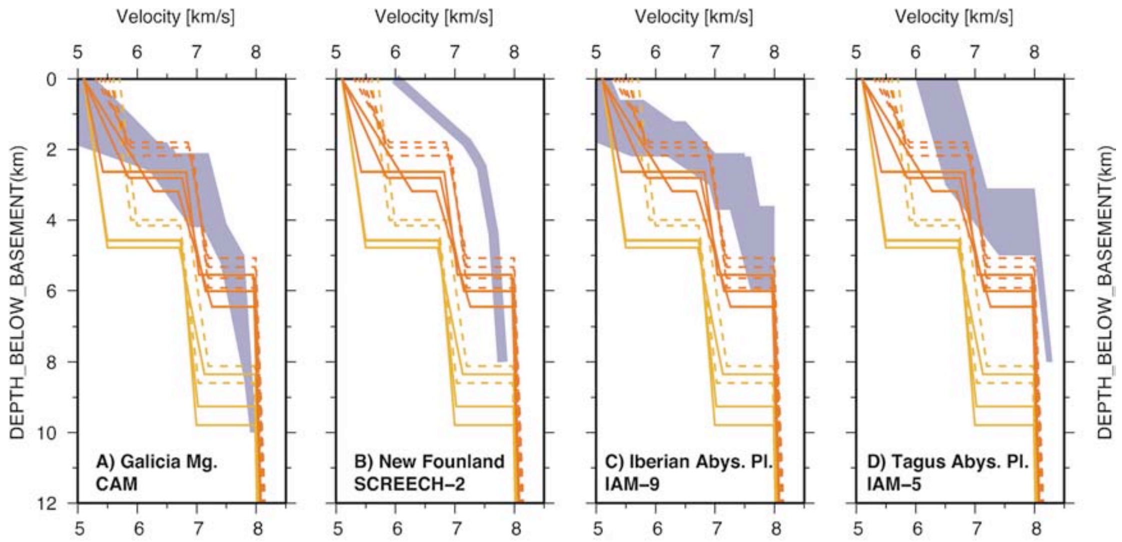

Figure 12 - Sardinia Sarde

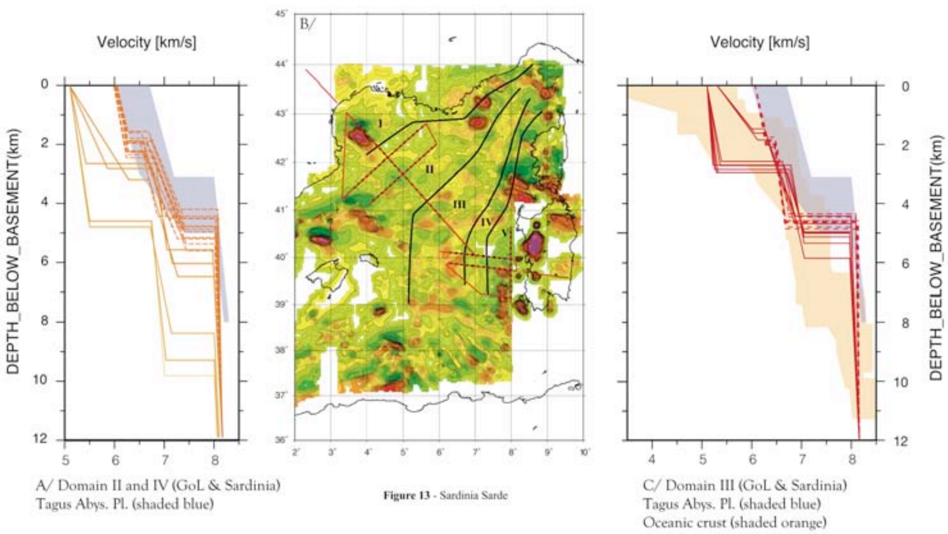

Figure 13 - Sardinia Sarde

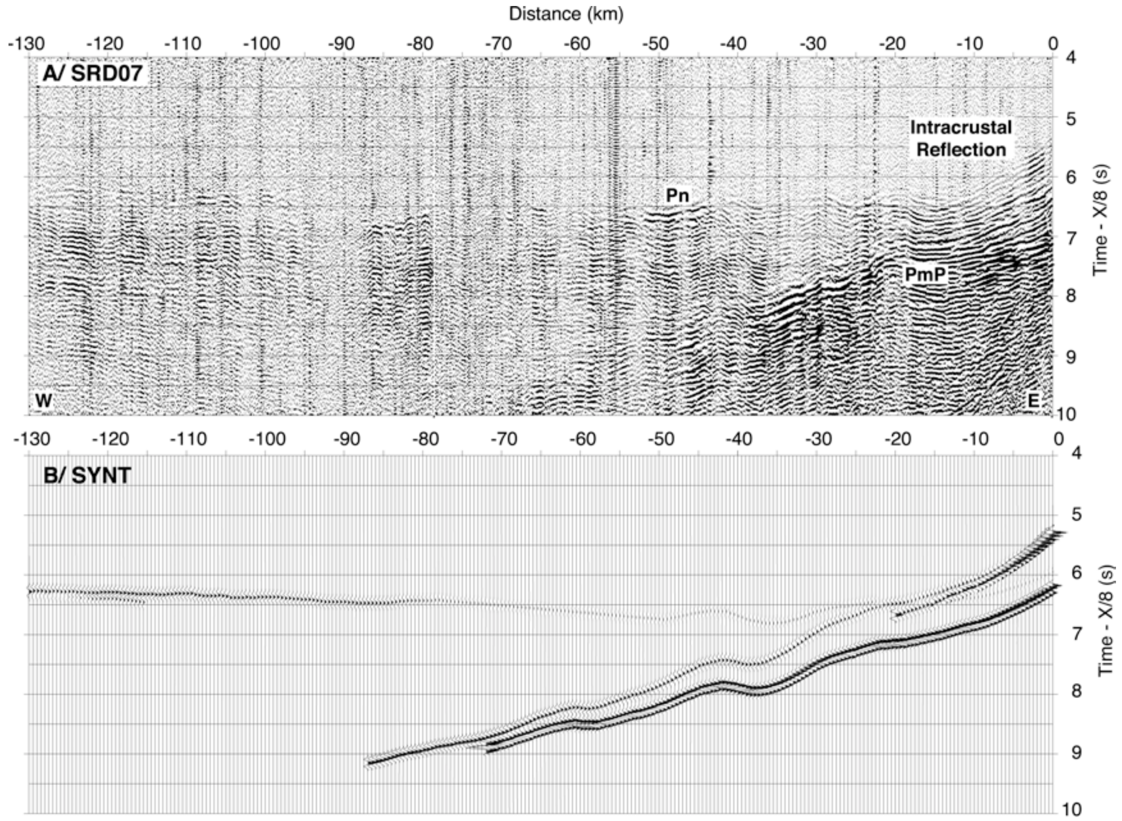

Figure Annex1 - Sardinia SARDE

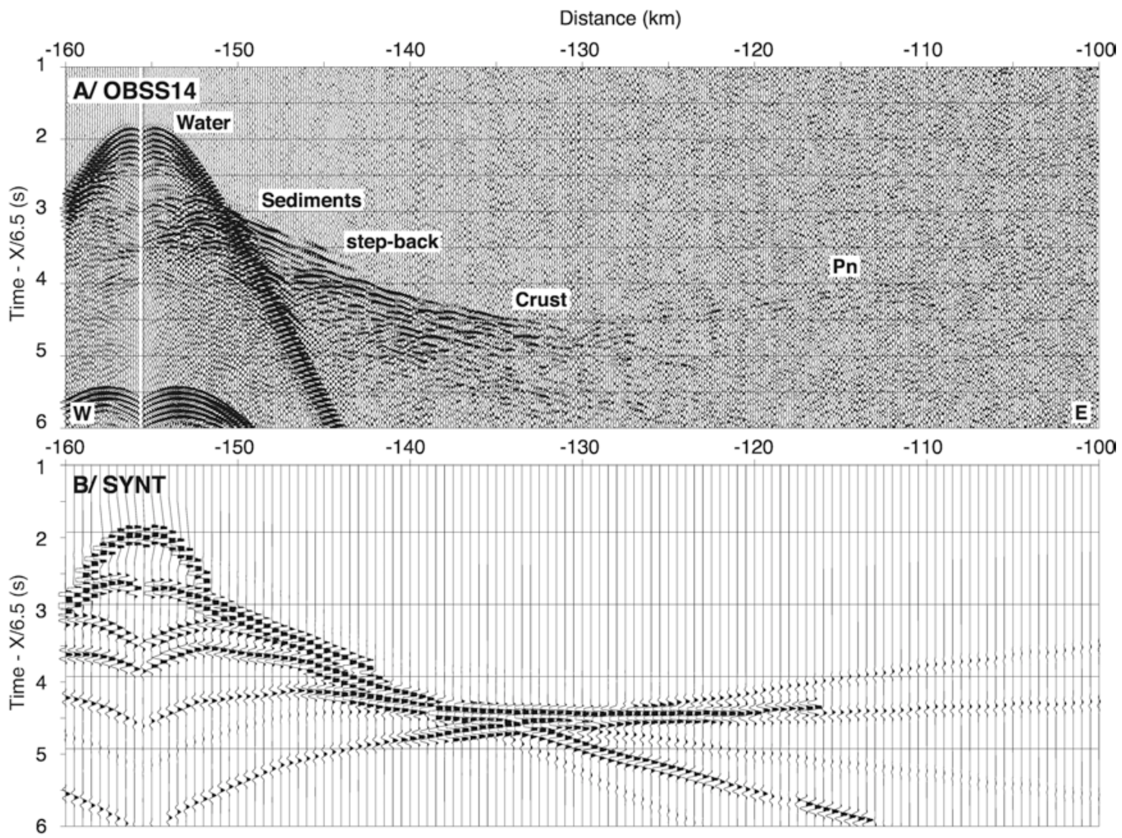

Figure Annex-2 - Sardinia SARDE

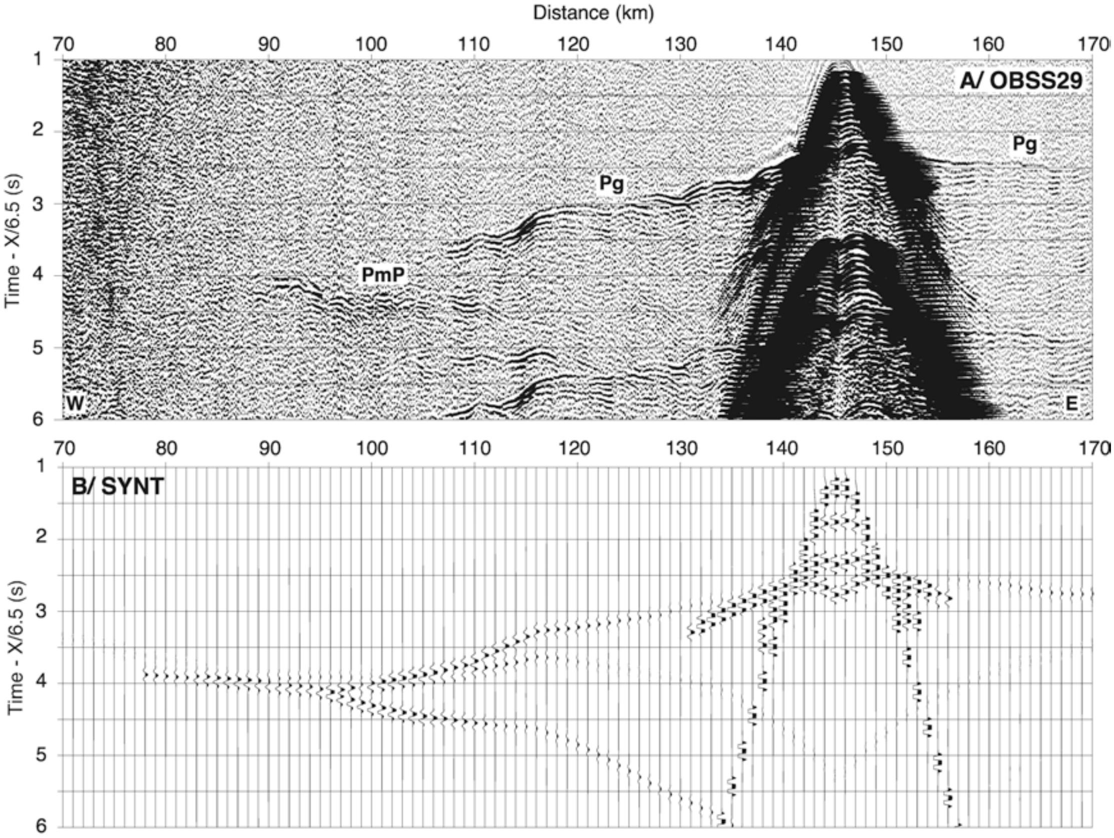

Figure Annex-3 - Sardinia SARDE

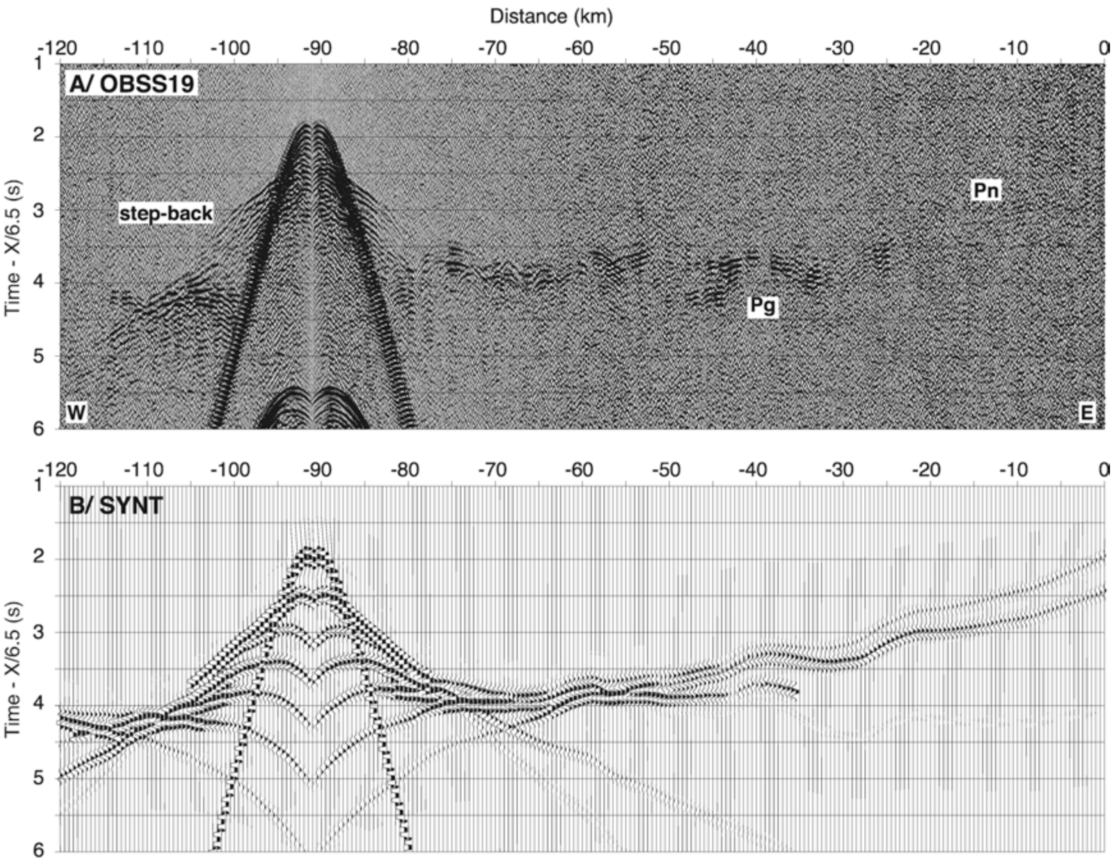

Figure Annex4 - Sardinia SARDE

TABLE I. – Travel-time residuals and chi-squared error for all phases and the complete model of profile GH.

Sardinia GH

Phase	No of Picks	RMS travel-time residual	Chi-squared
Water (Pw)	544	0.026	0.120
Top Salt (P3)	431	0.038	0.263
Top Salt reflection (P2P)	324	0.041	0.300
Base Salt reflection (P3P)	440	0.058	0.604
Sediments 3 (P5)	475	0. 062	0.683
Sediments 3 reflection (P4P)	475	0.062	0.683
Basement refraction (P6)	657	0.120	2.565
Basement Head wave (P6h)	688	0,122	2.667
Basement reflection (P5P)	497	0.074	0.977
Lower crust (P7)	793	0.087	1.337
Lower crust reflection (P6P)	404	0.068	0.816
PmP	1949	0.105	1.971
Pn	1264	0.116	2.404
All phases	8466	0.093	1.551

TABLE II. – Travel-time residuals and chi-squared error for all phases and the complete model of profile G_2H_2.

Sardinia G_2H_2

Phase	No of Picks	RMS travel-time residual	Chi-squared
Water (Pw)	4243	0.012	0.026
Sediments 2 (P3)	131	0.032	0.179
Sediments 3 reflection (P3P)	505	0.042	0.316
Top Salt reflection (P4P)	163	0.038	0.254
Salt / Sediments 3 (P5)	697	0.053	0.505
Base Salt reflection (P5P)	106	0.059	0.624
Sediments 3 reflection (P6P)	182	0.079	1.111
Sediments 4	14	0.025	0.120
Basement reflection (P7P)	666	0.060	0.643
Basement (P7)	931	0.082	1.195
Lower crust reflection (P8P)	108	0.186	6.184
Lower crust (P8)	392	0.084	1.272
PmP	394	0.157	4.406
Pn	343	0.096	1.659
All phases	8881	0.061	0.671